



Geochemical characteristics of gold bearing boninites and banded iron formations from Shimoga greenstone belt, India: Implications for gold genesis and hydrothermal processes in diverse tectonic settings

Sohini Ganguly ^a, C. Manikyamba ^{b,*}, Abhishek Saha ^{b,c}, M. Lingadevaru ^d, M. Santosh ^e, S. Rambabu ^b, Arubam C. Khelen ^b, D. Purushotham ^b, D. Linga ^b

^a Department of Geology, Andhra University, Visakhapatnam 530003, India

^b National Geophysical Research Institute (Council of Scientific and Industrial Research), Uppal Road, Hyderabad 500007, India

^c National Institute of Oceanography (Council of Scientific and Industrial Research), Regional Centre, Visakhapatnam 530017, India

^d Department of Geology, Central University of Karnataka, Gulbarga, India

^e School of Earth Science and Resources, China University of Geosciences, Beijing, China



ARTICLE INFO

Article history:

Received 30 July 2015

Received in revised form 10 October 2015

Accepted 12 October 2015

Available online 22 October 2015

Keywords:

Shimoga greenstone belt

Boninites

Banded iron formations

Gold

Hydrothermal fluids

Arc-continent collision

ABSTRACT

This paper is the first documentation of boninites from the Kudrekonda Formation of Shimoga greenstone belt (SGB) in western Dharwar Craton (WDC), India and the occurrence of native gold in the associated quartz veins. We also investigate the gold mineralization hosted in the banded iron formations (BIFs) of Ganajur, Karajgi and Palavanahalli areas of the SGB. The Kudrekonda metavolcanic rocks are composed of clinopyroxene, orthopyroxene and plagioclase with secondary amphibole. The geochemical attributes of these rocks, based on MgO, TiO₂, Ni, Cr and Co contents, Al₂O₃/TiO₂, (Gd/Yb)_N and (La/Sm)_N ratios, classify them as boninites and their relative LILE-HFSE abundance suggests magma generation in an intraoceanic arc setting. The Gd/Yb and Dy/Yb ratios suggest parent magma origin through partial melting of a spinel lherzolite mantle source. Geochemical signatures of the boninites suggest high temperature, shallow level melting of refractory mantle wedge metasomatized by fluids derived through dehydration of oceanic slab during subduction initiation. Quartz veins present in the Kudrekonda boninites contain gold grains showing affinity towards quartz-carbonate vein type greenstone hosted occurrences. EPMA data record 88.5–90.3 wt.% Au content with 7.7–8.4 wt.% Fe, 0.05–2.1 wt.% S and negligible Ag. The Au is hosted in Fe-oxides. Bulk chemical analyses show 4.1–684.4 ppb Au and 139.4–2186.4 ppb Ag in the studied samples. The gold mineralization of Kudrekonda boninites is syngenetic, mesothermal, convergent margin orogenic type. Decarbonation, desulphidization and metamorphism of subducted oceanic lithosphere and devolatilization of metasomatized enriched mantle wedge in intraoceanic arc setting are the viable processes that contributed to gold genesis in the Kudrekonda boninites. Devolatilization during prograde metamorphism, hydrothermal fluid generation, syntectonic gold remobilization and migration of gold enriched fluids through shear zones account for Au transportation and precipitation in quartz veins emplaced within the boninites. The BIFs of Ganajur, Karajgi and Palavanahalli areas of Shimoga greenstone belt dominantly comprise alternating Si-rich layers of quartz and Fe-rich hematite and magnetite layers. Geochemical characteristics of the BIF samples including their depleted ΣREE, positive Eu anomalies, negative to negligible Ce anomalies, and superchondritic Y/Ho ratios suggest that the BIFs were (i) derived by chemical sedimentation from paleo-ocean enriched in dissolved iron and silica with marked contributions from hydrothermal fluids of volcanic origin, and (ii) deposited in an off-shelf marine environment proximal to a mid-oceanic spreading centre where hydrothermal activity induced release of Eu and Y enriched hydrothermal solutions under low oxygen fugacity conditions. Native gold occurs in banded strata-bound disseminated sulphide lenses compositionally characterized as pyrite, arsenopyrite, chalcopyrite and galena. Mineral chemical analyses reveal 73–100% Au content with variable concentrations of Ag (0.02–15.2 wt.%). Geochemical compositions of BIFs are characterized by pronounced enrichment in Au (706–15,831 ppb) and Ag (630–2435 ppb). Gold mineralization in Shimoga BIFs is epigenetic, epithermal type akin to Homestake type iron-formation hosted vein and disseminated lode gold deposit. Gold genesis in these BIFs is attributed to migration of oxygen depleted, reducing, sulphidic-auriferous fluids of hydrothermal origin to the site of BIF deposition that served as chemical traps for the auriferous fluids. The Kudrekonda boninites represent accretion and preservation of a slice of older oceanic crust onto a relatively younger, active continental margin through arc-continent collision during Neoproterozoic time.

© 2015 Elsevier B.V. All rights reserved.

* Corresponding author.

E-mail address: cmaningri@gmail.com (C. Manikyamba).

1. Introduction

The Neoarchean period (2.7 Ga), marked by a peak in crustal growth, development of volcano-sedimentary greenstone sequences, komatiite-basalt volcanism, large scale deposition of banded iron formations (BIFs), cratonization, regional deformation and metamorphism, development of shear zone systems, generation of deep-seated hydrothermal fluids, remobilization and mineralization of precious metals, represents an important timeframe in the geological evolution of Archean shield areas (Isley and Abbott, 1999). The Archean cratons and late Neoproterozoic–Phanerozoic fold belts around the world are characterized by a variety of mafic and felsic igneous rocks and sediments including BIFs that host mesothermal orogenic gold deposits (Zhai and Santosh, 2013; Goldfarb and Santosh, 2014). The geological and geodynamic settings, nature of host rocks, structural control, depth of formation, ore–fluid oxidation state are the key parameters that control gold mineralization (Robert et al., 1997; Groves et al., 1998; 2005). On the basis of their geodynamic setting, gold deposits over the globe have been classified as convergent margin orogenic, continental margin to intracratonic Carlin type, arc related epithermal gold–silver deposits, oceanic arc to continental arc copper–gold porphyry deposits, orogenic to late orogenic iron oxide copper gold deposits and gold rich submarine volcanic hosted massive sulphide (VMS) to sedimentary exhalative (SEDEX) deposits (Kerrick et al., 2000; Li and Santosh, 2013; Guo et al., 2013; Groves and Santosh, 2015).

The concentration of orogenic gold deposits at 2.8–2.55 Ga, 2.1–1.75 Ga and 750–735 Ma corresponds to well defined periods of lithospheric growth at continental margins. This contention is consistent with the fact that gold mineralization is associated with addition of new oceanic lithosphere onto older cratonic margins through mantle plume activity and subduction accretion events (Condie, 2000; Kerrich et al., 2000; Groves et al., 2005). The metallogenesis of orogenic gold mineralization associated with Archean granite–greenstone terranes is primarily controlled by structural style, tectonic setting, metamorphism of host and associated rocks, timing of mineralization with respect to metamorphism and intrusive activity, alteration geochemistry, shear zone activity, hydrothermal system involving physico-chemical processes and flow of hydrothermal fluids for mobilization, transportation and deposition of gold (Goldfarb et al., 2001; Groves et al., 2003). Gold deposits hosted in metasedimentary rocks have spatial and temporal association with collisional orogens and are referred to as synorogenic gold deposits. The widespread distribution of these deposits throughout the accreted terranes of western North America suggests a direct association between continental growth and ore genesis (Barley et al., 1989; Kerrich and Wyman, 1990). Gold ores have formed both in interior orogens developed between large land masses during continent–continent collision (Appalachian–Caledonian, Hercynian, Uralian) and in peripheral orogens built during subduction of oceanic crust along continental margins (Cordilleran, Tasman). Collisional tectonic activities trigger crustal heating that is critical for devolatilization reactions and ore fluid formation (Powell et al., 1991; Phillips, 1991; Goldfarb et al., 1993). Transform movements along major crustal fault zones, contemporaneous or subsequent to heating also play a vital role for ore-forming process leading to relaxation of regional compressive forces and enhanced crustal-scale permeabilities. In many Phanerozoic belts, however, subordinate mafic volcanic rocks are interbedded with slates and graywackes which reflect contemporaneous sedimentation and oceanic arc or ridge volcanism prior to collision. Synorogenic mesothermal gold deposits are predominantly hosted by oceanic sedimentary rocks and despite a wide range in *P-T* of ore formation, these are widely-distributed in accreted terranes.

In India, gold mineralization has been documented from a wide variety of litho-assemblages such as i) lode gold occurring in quartz-carbonate veins of metamorphosed volcanic rocks of Archean greenstone belts, such as the gold mineralization in Kolar and Huttī, Ramagiri-Penakacherla, Gadag and Ajjanahalli greenstone belts of Dharwar Craton

(Manikyamba, 2000; Manikyamba et al., 2004; Pal and Mishra, 2004); ii) gold and associated sulphides in Neoarchean BIFs, such as the gold mineralization in Shimoga, Chitradurga and Sandur greenstone belts of Dharwar Craton (Manikyamba et al., 1997; Naqvi et al., 1998; 1999), Sonadehi in Madhya Pradesh; iii) vein and stratiform type gold deposits in southern granulite terrain (SGT), as exemplified by the Wyanad region of Kerala; iv) disseminated gold occurring in extrusive and intrusive igneous rocks, as represented by the Malanjkhand in Madhya Pradesh; v) gold in association with base metals like copper, lead, zinc occurring in Proterozoic volcanogenic polymetallic sulphide deposits, as seen in Khetri in Rajasthan, Rakha in Bihar; vi) detrital gold occurring in quartz-pebble conglomerates and quartzites, e.g. Dhanjori in Bihar, Bababudan in Karnataka, Cuddapah in Andhra Pradesh, vii) gold occurring in greywacke or turbidites of Neoarchean sedimentary successions along with volcanic intercalations e.g. Gadag in Karnataka; viii) detrital gold occurring in river alluvium and placers; and ix) gold occurring in laterites, soil and weathering profiles e.g. Nilambur valley in Kerala (Santosh and Omana, 1991). Gold mineralization in metabasalts, felsic volcanic rocks and banded iron formation is known from various greenstone belts of Dharwar Craton.

In the present paper, we report for the first time gold mineralization in the boninites of Kudrekonda, and document their geochemical characteristics based on which we evaluate the genesis of gold. We also discuss the gold mineralization hosted in BIFs from Ganajur, Karajgi and Palavanahalli areas of Shimoga greenstone belt in western Dharwar Craton (WDC). This paper reports boninites for the first time from the Shimoga greenstone belt in WDC and present the mineral chemical and whole rock geochemical data of gold bearing lithologies from these regions to address their genesis and evaluate the role in crustal growth and tectonic evolution of Shimoga greenstone belt.

2. Geological setting

The granite greenstone associations and intrusive granitoids of Dharwar Craton in southern peninsular India comprise a vast section of Meso-Neoarchean continental crust and range in age from 3.4 to 2.5 Ga (Swami Nath and Ramakrishnan, 1981; Naqvi and Rogers, 1987; Naqvi, 2005; Ramakrishnan and Vaidyanadhan, 2010; Jayananda et al., 2006, 2013a,b; Yang et al., 2014). The broad lithological components of the Dharwar Craton are represented by 3.36–2.7 Ga tonalite-trondhjemite–granodiorite (TTG) Peninsular gneisses, two generations of volcano-sedimentary sequences of 3.3–3.1 Ga Sargur Group and 2.9–2.5 Ga Dharwar Supergroup greenstone belts and 2.6–2.51 Ga calc-alkaline to potassic granitoid plutons (Chadwick et al., 2000; Moyen et al., 2003; Jayananda et al., 2008; Chardon et al., 2011; Fig. 1A inset).

The volcano-sedimentary sequences of 2.9–2.6 Ga Dharwar Supergroup are exposed in Bababudan, Chitradurga and Shimoga greenstone belts (Fig. 1A). The Bababudan Group includes oligomictic conglomerate, quartzite, phyllite, mafic–felsic volcanic rocks, tuffs and thick sequence of BIFs. The mafic volcanic rocks of Bababudan Group have an Sm–Nd whole rock isochron age of 2.9–2.8 Ga (Kumar et al., 1996) and zircons from felsic volcanic tuffs yield 2.2 Ga age (Trendall et al., 1997a,b). The Chitradurga Group comprises polymictic conglomerates, greywackes, argillites and limestones with intercalations of mafic–felsic volcanic rocks and BIFs (Chadwick et al., 1991). In general, the greenstone belts of WDC consists of ultramafic–mafic sequences, basalt–andesite–dacite–rhyolite (BADR), banded iron and manganese Formations, cherts, conglomerates, quartzites, greywackes and phyllites (Fig. 1A). The Dharwar Supergroup greenstone belts also consist of subordinate komatiites and komatiitic basalts besides predominant mafic–felsic volcanic rocks (Chadwick et al., 1991; Naqvi, 2005; Manikyamba et al., 2013, 2014a,b). The Shimoga greenstone belt is divided into Jhandimatti, Joldhal, Medur and Ranibennur Formations (Harinatha Babu et al., 1981; Fig. 1B). Detailed studies by Chadwick et al. (1991) have divided the Dharwar Supergroup rocks occurring adjacent to the Honnali dome of the Shimoga greenstone belt into three stratigraphic units viz.

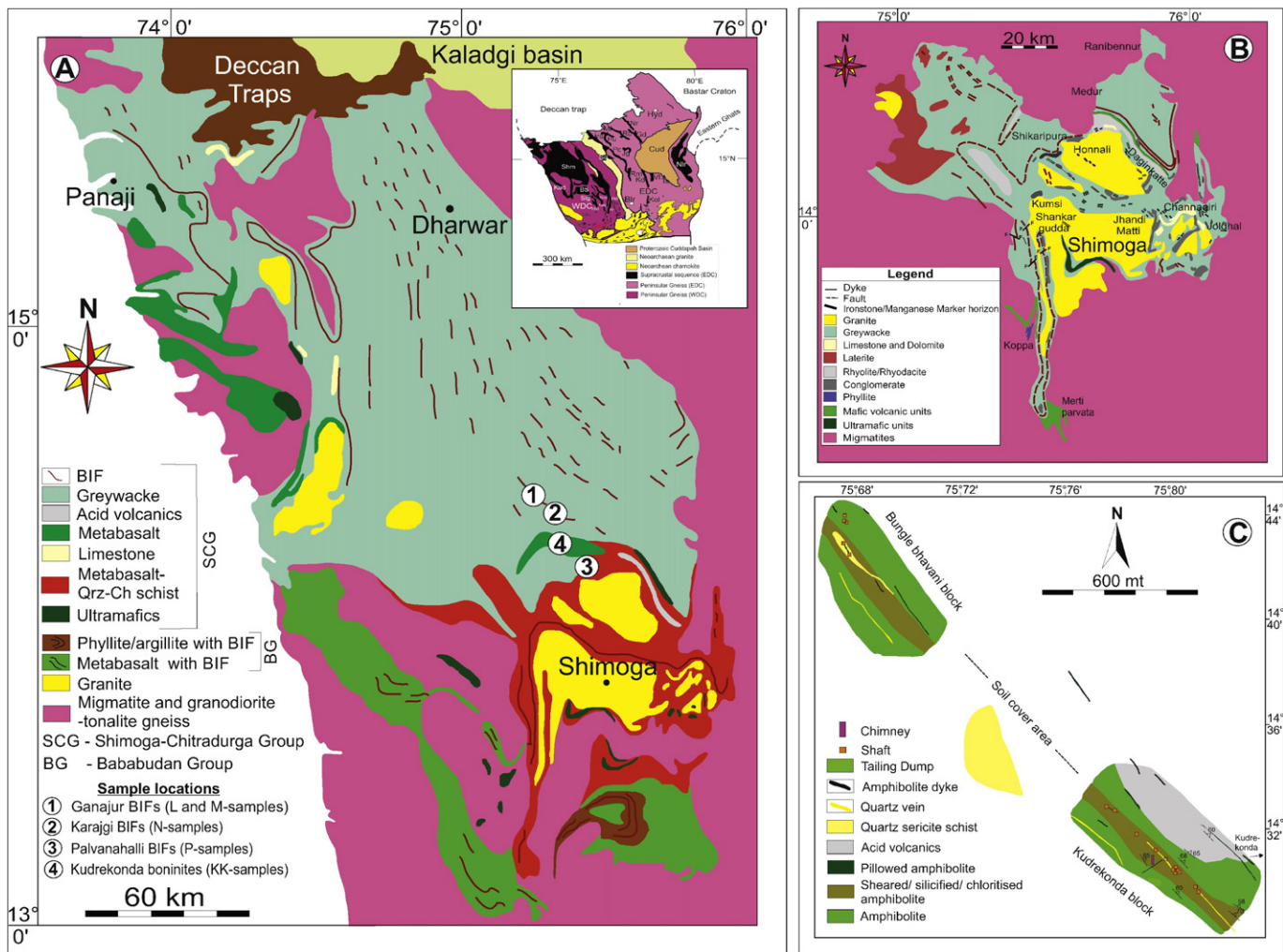


Fig. 1. (A) Geological map of western Dharwar Craton (WDC) showing Shimoga greenstone terrane and overall lithological associations of Shimoga–Chitradurga and Bababudan Groups. Sample locations of present study are given. Inset: Simplified geological map of southern Peninsular India showing the western and eastern sectors of Dharwar Craton with the intervening belt of Closepet granites and the distribution of greenstone terranes. (B) Geological map of Shimoga greenstone terrane (modified after Harinadha Babu et al. (1981)). (C) Simplified geological map of Kudrekonda showing auriferous quartz veins cutting across the amphibolites.

the Bababudan Group, the lower and upper Chitradurga Groups. The Bababudan Group comprises a sequence of metabasalt–orthoquartzite that has been subdivided into Kudrekonda and Kalvarangandurga Formations. The Bababudan Group is overlain by a lithological association of polymictic conglomerate and limestone interlayered with mafic and felsic volcanic rocks representing the lower Chitradurga Group which has been subdivided into Musinhal, Adrihalli, Aleshpur, Medur and Daginkatte Formations (Fig. 1B). These are followed by the upper Chitradurga Groups including Basavapatna and Ranibennur Formations. The rocks of Shimoga greenstone belt show evidence of pervasive low grade greenschist facies metamorphism with relatively higher grade greenschist–amphibolite transition facies located along particular tectonic axis. The overall mineralogical assemblage reflects regional metamorphism spanning from lower greenschist (chlorite–biotite) to upper greenschist–amphibolite facies (Swami Nath and Ramakrishnan, 1981). There is no geochronological data available till date on the mafic volcanic rocks of Kudrekonda. However, the felsic volcanic rocks of the Daginkatte Formation have been dated at 2614 ± 5 Ma reflecting on Neoarchean age (Trendall et al., 1997a).

The Honnali dome, situated in the Shimoga greenstone belt of WDC, is lithologically composed of metamorphosed volcanosedimentary sequences and is characterized by extensive old workings for gold that has particularly designated the area as Honnali gold field. An auriferous

zone of 10 km length and 2 km width occurs at 15–16 km south-west of Honnali dome. Investigations carried out by State Department of Mines and Geology and reports by Radhakrishna (1940, 1941), Rama Rao (1963) and Radhakrishna and Curtis (1991) have documented placer and alluvial gold in Kudrekonda, Palavanahalli and Budigere areas located in this auriferous zone of Honnali dome (Fig. 1A). Recently, three discontinuous, NNW–NW trending, parallel auriferous quartz veins have been documented by Lingadevaru (2007). These quartz veins occur within highly deformed amphibolites of Kundrekonda (Fig. 1C) and the mineralized zone comprises fine specks of native gold associated with sulphides like chalcopyrite, arsenopyrite, sphalerite, pyrrhotite and covellite. In Kudrekonda area, Au values estimated by fire assay method spanning between 0.2 and 2.4 g/t. Quartz and amphibolites of Pallavanahalli contain 0.2–0.8 g/t Au, while quartz with sheared silicified and carbonated amphibolites from the same area have been examined for 0.2–3.2 g/t Au (Lingadevaru, 2007). The Ganajur, Karajgi and Palavanahalli areas, located north and northwest of the Honnali dome of Shimoga greenstone belt, are characterized by cherty and sulphidic banded iron formations which are auriferous and associated with deeply weathered greywackes (Fig. 1A). A well developed zone of conglomerate and quartzite forms the southwestern extent of the Honnali dome where old workings are located at the foot of the Kalavaranganetta mountain range (Radhakrishna and Curtis, 1999).

Table 1

Major and trace element concentrations of UB-N and JB-2 obtained from XRF and HR-ICP-MS.

wt.%	A	B	SD	%RSD	A	B	SD	%RSD
UB-N								
SiO ₂	39.47	39.43	0.03	0.07	53.24	53.20	0.03	0.05
Al ₂ O ₃	2.77	2.90	0.09	3.32	14.66	14.67	0.01	0.05
Fe ₂ O ₃	8.32	8.34	0.01	0.17	14.36	14.34	0.01	0.10
MnO	0.12	0.12	0.00	0.00	0.20	0.20	0.00	0.00
MgO	35.31	35.21	0.07	0.20	4.68	4.66	0.01	0.30
CaO	1.21	1.20	0.01	0.58	9.78	9.89	0.08	0.80
Na ₂ O	0.10	0.10	0.00	0.00	2.01	2.03	0.01	0.70
K ₂ O	0.02	0.02	0.00	3.37	0.41	0.42	0.01	1.72
TiO ₂	0.11	0.11	0.00	1.26	1.21	1.19	0.01	1.17
P ₂ O ₅	0.04	0.04	0.00	1.72	0.10	0.10	0.00	0.00
ppm								
Sc	14.138	13	0.584	4.287	54.213	54.4	0.809	1.492
V	77.908	75	3.181	3.866	533.909	578	44.634	8.360
Cr	2442.546	2300	156.296	6.322	26.485	27.4	2.411	9.104
Co	104.663	100	8.108	7.910	39.756	39.8	0.664	1.671
Ni	2048.329	2000	68.092	3.325	14.028	14.2	0.269	1.920
Cu	28.527	28	2.053	7.151	225.935	227	4.829	2.137
Zn	92.122	85	3.872	4.453	112.408	110	5.331	4.743
Ga	3.065	3	0.043	1.400	17.284	17	0.320	1.850
As	3.002	2.98	0.086	2.855	11.900	11.4	0.354	3.032
Rb	4.293	4	0.316	7.778	6.214	6.2	0.155	2.495
Sr	9.065	9	0.321	3.556	180.528	178	4.072	2.256
Y	2.596	2.5	0.224	9.044	25.261	24.9	0.701	2.773
Zr	3.752	4	0.296	7.512	52.405	51.4	1.945	3.712
Nb	0.049	0.05	0.004	7.358	0.804	0.8	0.034	4.286
Cs	9.715	10	0.558	5.478	0.895	0.9	0.012	1.315
Sb	0.267	0.27	0.005	1.908	0.323	0.3	0.022	7.530
Ba	26.018	27	1.173	4.238	207.804	208	3.329	1.602
La	0.338	0.35	0.010	2.865	2.376	2.37	0.046	1.931
Ce	0.841	0.8	0.058	7.264	6.842	6.77	0.106	1.544
Pr	0.121	0.12	0.008	7.020	0.972	0.96	0.021	2.119
Nd	0.591	0.6	0.042	6.990	6.750	6.7	0.245	3.634
Sm	0.200	0.2	0.012	5.951	2.255	2.25	0.100	4.456
Eu	0.088	0.08	0.007	8.950	0.883	0.86	0.031	3.563
Gd	0.321	0.3	0.017	5.683	3.316	3.28	0.111	3.346
Tb	0.064	0.06	0.006	9.542	0.626	0.62	0.015	2.419
Dy	0.369	0.38	0.018	4.689	3.695	3.66	0.104	2.804
Ho	0.096	0.09	0.008	8.292	0.806	0.81	0.019	2.377
Er	0.281	0.28	0.020	7.490	2.644	2.63	0.081	3.049
Tm	0.044	0.045	0.002	4.040	0.451	0.45	0.013	2.940
Yb	0.275	0.28	0.019	6.661	2.547	2.51	0.100	3.923
Lu	0.047	0.045	0.003	5.469	0.398	0.39	0.012	2.990
Hf	0.102	0.1	0.004	4.351	1.503	1.42	0.036	2.366
Ta	0.021	0.02	0.001	3.541	0.214	0.2	0.013	6.181
Pb	12.160	13	0.685	5.344	5.259	5.4	0.535	10.182
Th	0.075	0.07	0.006	8.933	0.333	0.33	0.018	5.421
U	0.076	0.07	0.005	7.115	0.160	0.16	0.008	4.943
FER-1								
SiO ₂	16.91	16.92	0.01	0.04	49.22	49.24	0.01	0.03
Al ₂ O ₃	0.51	0.50	0.01	1.39	5.22	5.20	0.01	0.27
Fe ₂ O ₃	75.70	75.72	0.01	0.02	39.42	39.40	0.01	0.04
MnO	0.23	0.22	0.01	3.07	0.12	0.12	0.00	0.00
MgO	0.27	0.28	0.01	2.62	2.11	2.10	0.01	0.34
CaO	3.30	3.31	0.01	0.21	2.22	2.20	0.01	0.64
Na ₂ O	0.01	0.01	0.00	0.00	0.46	0.47	0.01	1.54
K ₂ O	0.01	0.01	0.00	0.00	1.32	1.33	0.01	0.54
TiO ₂	0.03	0.03	0.00	2.44	0.18	0.19	0.01	3.93
P ₂ O ₅	2.45	2.44	0.01	0.29	0.26	0.27	0.01	2.72
ppm								
Sc	0.578	0.87	0.085	14.770	3.017	6	0.074	2.451
V	103.429	98	1.791	1.732	44.801	36	0.585	1.307
Cr	7.247	7	0.159	2.194	6.521	46	0.037	0.575
Co	12.020	12	0.313	2.600	5.724	7	0.023	0.407
Ni	10.476	12	0.128	1.226	1.772	25	0.018	1.013
Cu	102.145	105	0.854	0.836	0.483	47	0.002	0.475
Zn	3573.270	3600	28.555	0.799	19.280	44	0.168	0.870
Ga	2.586	1.75	0.117	4.537	7.144	1	0.091	1.279
As	8.970	7	0.267	2.979	0.136	1	0.002	1.293
Rb	0.619	0.6	0.004	0.622	59.866	67	0.643	1.074
Sr	97.639	90	1.246	1.276	55.322	58	0.006	0.010
Y	19.223	18	0.073	0.380	15.664	0.16	0.016	0.104
Zr	6.369	6	0.516	8.101	114.776	39	0.140	0.122
Nb	1.032	1	0.007	0.641	5.212	1	0.020	0.393
Cs	0.825	1	0.052	6.330	8.044	4.5	0.032	0.396

Table 1 (continued)

wt.%	A	B	SD	%RSD	A	B	SD	%RSD
Sb	8.843	6	0.627	7.088	0.002	1	3.13	0.345
Ba	1114.647	1000	18.630	1.671	236.975	230	0.029	0.012
La	10.506	9.8	0.054	0.511	14.094	12	0.016	0.114
Ce	8.060	7.5	0.032	0.403	28.517	25	0.023	0.079
Pr	1.704	1.55	0.021	1.212	3.187	3	0.013	0.408
Nd	7.781	7	0.108	1.386	13.437	12	0.112	0.836
Sm	1.881	1.7	0.030	1.580	2.663	2.5	0.032	1.214
Eu	3.376	3.1	0.070	2.059	1.283	1.25	0.012	0.973
Gd	1.632	1.5	0.069	4.207	2.018	2	0.010	0.500
Tb	0.206	0.2	0.005	2.439	0.417	0.32	0.009	2.227
Dy	1.840	1.8	0.033	1.799	2.416	2	0.000	0.017
Ho	0.409	0.4	0.008	1.868	0.288	0.6	0.002	0.684
Er	1.024	1	0.021	2.003	0.966	1.5	0.005	0.475
Tm	0.194	0.2	0.001	0.708	0.178	0.2	0.002	0.898
Yb	1.009	0.98	0.014	1.375	1.341	1.25	0.013	0.972
Lu	0.157	0.15	0.003	2.159	0.224	0.2	0.001	0.226
Hf	0.239	0.12	0.022	9.246	2.885	1	0.031	1.070
Ta	0.041	0.024	0.003	8.430	0.181	0.2	0.001	0.446
Pb	6061.108	5200	149.792	2.471	19.141	11	0.109	0.569
Th	0.412	0.4	0.007	1.614	2.870	2.4	0.034	1.176
U	0.606	0.6	0.015	2.550	1.174	1.2	0.004	0.361
CH3-1								
ppb	A	B	SD	%RSD	MA-1a			
	A	B	SD	%RSD	A	B	SD	%RSD
Ag	2585.9	2636	176.181	6.813	–	–	–	–
Au	1459.7	1400	65.004	4.453	21338.5	212000	1173.434	5.499

A: present study (average of five values); B: reorted values from Govindaraju GEOREM (georem.mpch-mainz.gwdg.de).

3. Sampling and analytical techniques

Samples of BIFs for the present study have been collected from the outcrops at Ganajur (L, M), Karajgi (N) and Palavanahalli (P) areas of Shimoga greenstone belt. The auriferous metavolcanic rocks (KK) and quartz vein samples have been collected from the regions of old workings at Kudrekonda. Thin sections of the samples were studied under optical microscope and Electron Microprobe Analyses (EPMA) of the constituent gold and sulphide phases from selected samples of BIFs and quartz vein bearing metavolcanic rocks were performed at EPMA LAB, NCEGR, Geological Survey of India, Bangalore using a four spectrometer CAMECA SX100 microprobe. Counts were obtained simultaneously using a 20 keV accelerating voltage, a 1 μm beam diameter, and a beam current of 20 nA. Natural and synthetic metal standards (having compositions Pyrite = Fe: 46.55%; S: 53.45%; Sphalerite = Zn: 67.1%; S: 32.9%; Au = Au: 99.999%; Ag = Ag: 100%; Cu = Cu: 100%; Co = Co: 100%; Ni = Ni: 100%; GaAs = Ga: 48.2%; As: 51.8%) were used for calibrations and the PAP correction was applied to the data.

For whole rock analyses, after petrographic screening, 54 samples (42 samples of BIF and 12 samples of boninites) were selected for major, trace including rare earth element (XRF and HR-ICPMS) and gold (Pb fire assay method) analysis. Selected samples of BIFs and metavolcanic rocks were powdered using planetary ball mill crusher. The powdered samples along with matrix matching geochemical reference materials were analysed for major, trace and REE compositions at National Geophysical Research Institute (NGRI), Hyderabad. Major element concentrations were determined by X-ray fluorescence spectrometry (XRF; Phillips MAGIX PRO Model 2440), on pressed pellets prepared from powdered whole-rock samples following the method of Krishna et al. (2007). The trace elements including rare earth elements (REE) were analysed by dissolving the sample powders followed closed digestion method of Manikyamba et al. (2014c). The samples were analysed at NGRI using high resolution inductively coupled mass spectrometer (HR-ICP-MS) (Nu Instruments Attom, UK) along international certified reference materials of UB-N, JB-2, Fer-1 and Fer-2. The details of the instrument and the analytical procedure are referred to Manikyamba et al. (2014c). Precision and reproducibility obtained for international reference materials are given in Table 1 which is found to be better than 2% RSD for majority of the trace elements. However, Arsenic (As) and Antimony (Sb) are semiquantitative.

Gold was analysed following the Pb Fire assay method in which 10 g of finely ground sample powder mixed with flux (Litharge ($PbO = 40\text{ g} + \text{Sodium Carbonate } (Na_2CO_3) = 30\text{ g} + \text{Potassium Carbonate } (K_2CO_3) = 5\text{ g} + \text{Borax } (NO_2B_4O_7) = 8\text{ g} + \text{Silica } (SiO_2) = 10\text{ g} + \text{flour } (C) = 2\text{ g}$) that are taken in a polythene cover. One ml of silver nitrate solution containing 5 mg Ag has been added to this mixture and thoroughly shaken for complete homogenization. Care was taken to avoid lumping of flux. The mixture was transferred to a preheated and cooled graphite crucible and kept for fusion in preheated muffle furnace at $1050 \pm 25^\circ\text{C}$ for one hour. The melt obtained after fusion was swirled and poured into an iron mould to which a thin oil film had been applied to the inner surface. The molten mass was cooled for 30 min and the lead button formed was separated from the slag by hammering. The lead button was cleaned and cupped in a bone ash crucible at $950 \pm 25^\circ\text{C}$ for one hour. The silver pril containing Au and PGE obtained after cupellation was weighed and dissolved in a 10 ml HNO_3 . In this process silver gets dissolved as silver nitrate ($AgNO_3$), the filtrate is decanted and the residue has been treated with aqua regia. 10 ml of concentrated HCl has been added to the filtrate to precipitate Ag as $AgCl$. The filtrate was then decanted and added to aqua regia solution. The volume of the Au and PGE containing solution was made up to 100 ml along with the addition of 10 ml of Thallium solution as an internal standard. The solutions were analysed for Au along with international reference materials CH-3 and Ma-1a (Table 1) on HR ICP-MS at NGRI, Hyderabad.

4. Ore petrography and chemistry

The Kudrekonda mafic volcanic rocks occur as subcrops which are chloritized and permeated by quartz and carbonate veins at some places (Fig. 2A). The BIFs of Ganajur have extensive outcrops in which spectacular box work is present at many places. Silicification, carbonatization and sulphidation are common features observed in the field (Fig. 2B). In BIFs from Karajgi area, crosscutting quartz veins occur at some places (Fig. 2C). The mineralogical composition of the Kudrekonda metavolcanic rocks is characterized by clinopyroxene, orthopyroxene and plagioclase (Fig. 2D) with biotite and opaques occurring as accessory phases. Amphiboles are secondary after clinopyroxene (Fig. 2D). The igneous mineralogy of the studied samples has been altered by greenschist to lower



Fig. 2. (A) Field photographs of (A) Kudrekonda boninites cut across by quartz and carbonate veins (B) Ganajur BIF showing sulphidization, carbonatization and box work structure (C) crosscutting quartz vein in the Karjagi BIF, (D) Photomicrograph showing occurrence of orthopyroxene (opx), plagioclase (pl) in Kudrekonda boninites. Amphibole (amp) is secondary after clinopyroxene and biotite (bt) occurs as accessory phase and (E) photomicrograph of BIF showing alternating Fe-rich and Si-rich bands.

amphibolite facies metamorphism. Primary igneous textures have been overprinted by an overall schistose texture. The studied samples contain numerous quartz veins that host gold mineralization. Alternating Si-rich and Fe-rich layers represent the most distinguishing petrographic feature of the BIF samples from Ganajur, Karjagi and Palavanahalli areas (Fig. 2E). The Si-rich layers are predominantly composed of quartz, while Fe-rich layers consist of haematite and magnetite. Disseminated sulphides occur as opaque phases. These BIFs have been also cut across by quartz veins at places.

Electron probe micro analyses of gold grains and associated sulphide minerals hosted in quartz veins of mafic volcanic rocks of Kudrekonda (KK) and BIFs of Ganajur (L, M) and Karjagi (N) areas of Shimoga greenstone belt are given in Table 2. In the analysed gold grains from Kudrekonda, Au content ranges from 88.5 to 90.3 wt.% with Fe and S concentrations spanning from 7.7 to 8.4 and 0.05 to 2.1 wt.% respectively and negligible Ag. EPMA data of gold from Ganajur samples show

maximum Au content ranging from 72.9 to 100.3 wt%. Gold grain having Au content >99 wt.% is considered to be native gold. In the BIF samples, Au grains are hosted in Fe-oxides (Figs. 3A and B), while in Kudrekonda metavolcanic rocks, Au grains mostly occur within quartz vein (Figs. 3C and D). Mineral chemical compositions of BIF sample N11 show relatively higher Ag (14.5–15.2 wt.%) and Fe (9.3–11.1 wt.%) contents than that of sample N5 (Ag = 0.02–0.3 wt.%; Fe = 0.05–0.1) having feeble concentrations of Ag and Fe. Chemical compositions of gold from Karjagi BIFs are marked by a consistent range of Au (85.7–88.4 wt.%) with uniformly higher Ag (8.9–9.1 wt.%) forming a Au-Ag alloy (Figs. 3E and F). Ag concentration in gold grains from Karjagi is higher than that of the gold grains from Kudrekonda and Ganajur. In the Karjagi BIFs, gold grain occurs in association with quartz and Fe-oxides (Figs. 3G and H). EPM analyses of base metal sulphides occurring with gold in the studied BIF and quartz vein-hosted metavolcanic rocks are given in Table 3. In the BIF samples, the sulphide minerals occurring

Table 2
EPM analyses of gold grains from BIFs and boninites of Shimoga greenstone belt

	M1							N11							N5							KK8						
	wt%	1	2	3	4	5	6	7	1	2	3	4	5	6	7	8	1	2	3	4	5	6	7	8				
S	0.11	0.06	0.12	0.1	0.12	0.06	0.13	0.112	0.08	0.09	0.04	0.03	0.05	—	0.02	0.04	0.01	0.03	2.09	0.12	0.09	0.05	0.07	0.14	0.09	0.05		
Fe	0.69	0.56	0.58	2.04	1.39	0.53	0.51	11.11	10.8	9.29	0.09	0.08	0.05	0.08	0.13	0.07	0.1	0.14	8.13	8.39	7.87	8.11	7.69	8.33	7.94	8.43		
Co	0.02	0.05	—	0.02	—	0.01	—	0.03	—	0.32	0.2	0.3	0.36	0.37	0.3	0.23	0.39	—	—	—	—	—	—	—	—			
Ni	—	—	0.01	—	—	—	0.01	0.07	—	0.02	0.17	—	0.08	0.02	0.08	0.02	0.04	0.08	0.02	0.06	0.05	0.07	0.05	0.07	0.08			
Ag	9.02	9.12	9.04	9.14	8.94	9.12	8.99	14.54	15.07	15.21	—	—	0.04	0.02	—	—	0.34	0.11	—	—	0.02	0.02	—	—	—			
Au	88.12	88.42	88.4	85.74	87.46	87.52	87.33	74.6	72.86	75.67	100.29	100.28	100.1	98.54	95.68	99.02	96.97	96.21	88.54	89.53	90.34	90.17	90.22	89.97	89.63			
Cu	—	0.04	0.1	0.05	0.14	0.06	—	—	0.1	0.04	0.04	0.18	0.09	0.07	0.13	0.29	0.21	0.08	0.02	0.14	—	0.12	0.05	0.07	0.1			
As	—	—	—	—	0.02	—	—	—	—	—	—	—	—	—	—	—	—	—	—	—	0.01	—	—	—	—			
Total	97.96	98.25	98.25	97.09	98.07	97.3	97.18	100.44	98.94	100.3	100.8	100.94	100.63	99.15	96.35	99.8	97.94	96.98	98.82	98.27	98.36	98.49	98.05	98.17				

M1: Ganajur BIF.

N11 and N5: Karajgi BIF.

KK8: Kudrekonda boninite.

with gold are compositionally characterized as sphalerite, pyrite, arsenopyrite and chalcopyrite while sulphides in auriferous quartz veins of metavolcanic rocks correspond to sphalerite (Fig. 4A) and pyrite (Fig. 4B; Table 3). EPM analyses of sphalerite are marked by 49.9–58.5 wt.% Zn, 39.12–32.2 wt.% S and 6.8–10.5 wt.% Fe, while that of pyrite show 44.8–58.4 wt.% Fe and 40.1–54.03 wt.% S (Table 3). Mineral chemistry of arsenopyrite (Fig. 4C) is characterized by 43.04 wt.% As, 27.7–33.3 wt.% Fe and 18.03–19.9 wt.% S. In chalcopyrite (Fig. 4D) Cu ranges from 38.03 to 35.6 wt.% and S varies between 35.8 and 33.5 wt.% with Fe showing a range of 24.8–29.3 wt.% (Table 3). Galena also occurs as sulphide phase (Fig. 4E). Ag grain occurring within Fe-oxides has also been noted (Fig. 4F). Semi-quantitative analysis show ~69 wt.% Ag content in the grain (Fig. 4F inset).

5. Results

5.1. Geochemistry of volcanic rocks

The Kudrekonda metavolcanic rocks from Shimoga greenstone belt are characterized by a wide variation in SiO₂ contents ranging from 26.4 to 45.2 wt.% with low TiO₂ (0.1–0.75 wt.%), moderate to high Al₂O₃ (6–18 wt.%), moderate Fe₂O₃ (6.5–11.3 wt.%) contents, low to high CaO (0.2–24.2 wt.%), high MgO (22.1–30.5 wt.%) concentrations and consistently high Mg# (Mg# = 70–84; Table 4). The studied samples show low total alkali (0.1–4.4 wt.%) and P₂O₅ (0.02–0.11 wt.%) contents. On (Yb)_N vs. (Dy)_N diagram the studied samples occupy the field of boninites with a lone plot falling in the field of island arc tholeiite (Fig. 5A). On Cr vs. Y plot (Dilek and Furnes, 2009; Fig. 5B) these rocks clearly correspond to the boninite field. Immobile trace element concentrations like Ti, Zr, V, Sc and Yb serve as important tools for discriminating high Mg volcanic rocks like boninites, SHMB, low-Ti tholeiites, komatiites and komatiitic basalts (Rollinson, 1993; Smithies, 2002). The geochemical characteristics of the Kudrekonda boninites are clearly distinguishable from that of SHMB, komatiites, komatiitic basalts, MORB in terms of Ti, V, Sc and Yb. On Ti/V vs. Ti/Sc and Yb vs. Ti plots (Fig. 5C) most of the Kudrekonda samples occupy the fields of boninites except two samples corresponding to Paleoproterozoic high-Mg norite and one falling in the field of siliceous high-Mg basalts (SHMB).

These high MgO metavolcanic rocks are marked by typically high Al₂O₃/TiO₂ ratios ranging from 23.6 to 75.5 (except sample KK 10 having Al₂O₃/TiO₂ = 13.5) which attest to their boninitic affinity. Therefore, major, trace and REE compositions classify the studied Kudrekonda metavolcanic rocks as boninites. The Kudrekonda boninites characteristically exhibit high Al₂O₃/TiO₂ and CaO/TiO₂ ratios at low (Gd/Yb)_N and TiO₂ contents respectively. In terms of immobile trace element variations, these samples plot in the field of sub-alkaline basalt (Fig. 5D; Winchester and Floyd 1977). Based on CaO/Al₂O₃ ratios (Crawford, 1989), the studied samples have been classified as low-Ca (CaO/Al₂O₃ = 0.01–0.66) and high-Ca (CaO/Al₂O₃ = 0.83–3.12) boninites.

Among the transitional trace elements, the Kudrekonda boninites have variable concentrations of Ni (193–1580 ppm), Cr (246.73–7965.7 ppm) and Co (43.31–116.13 ppm). The Ni and Cr concentrations of some samples are higher than the primitive mantle values (Ni: >400 and Cr: >800 ppm). The trace element chemistry of the Kudrekonda boninites is marked by enriched LILE, LREE and depleted HFSE compositions. The studied samples exhibit characteristic U-shaped chondrite normalized REE patterns with distinct LREE and HREE enrichment and relative MREE depletion that resembles typical boninitic character (Fig. 6A). Primitive mantle normalized trace element abundances of these rocks depict negative anomalies at Nb, Ta, Zr and Hf (Fig. 6B). The Kudrekonda boninites have high concentrations of Ag (139.45–2186.38 ppb) and variable concentrations of Au (4.1–684.4 ppb; Table 4). A bar diagram (Fig. 7) shows relative distribution of gold (Au) and associated elements arsenic (As) and antimony (Sb) in

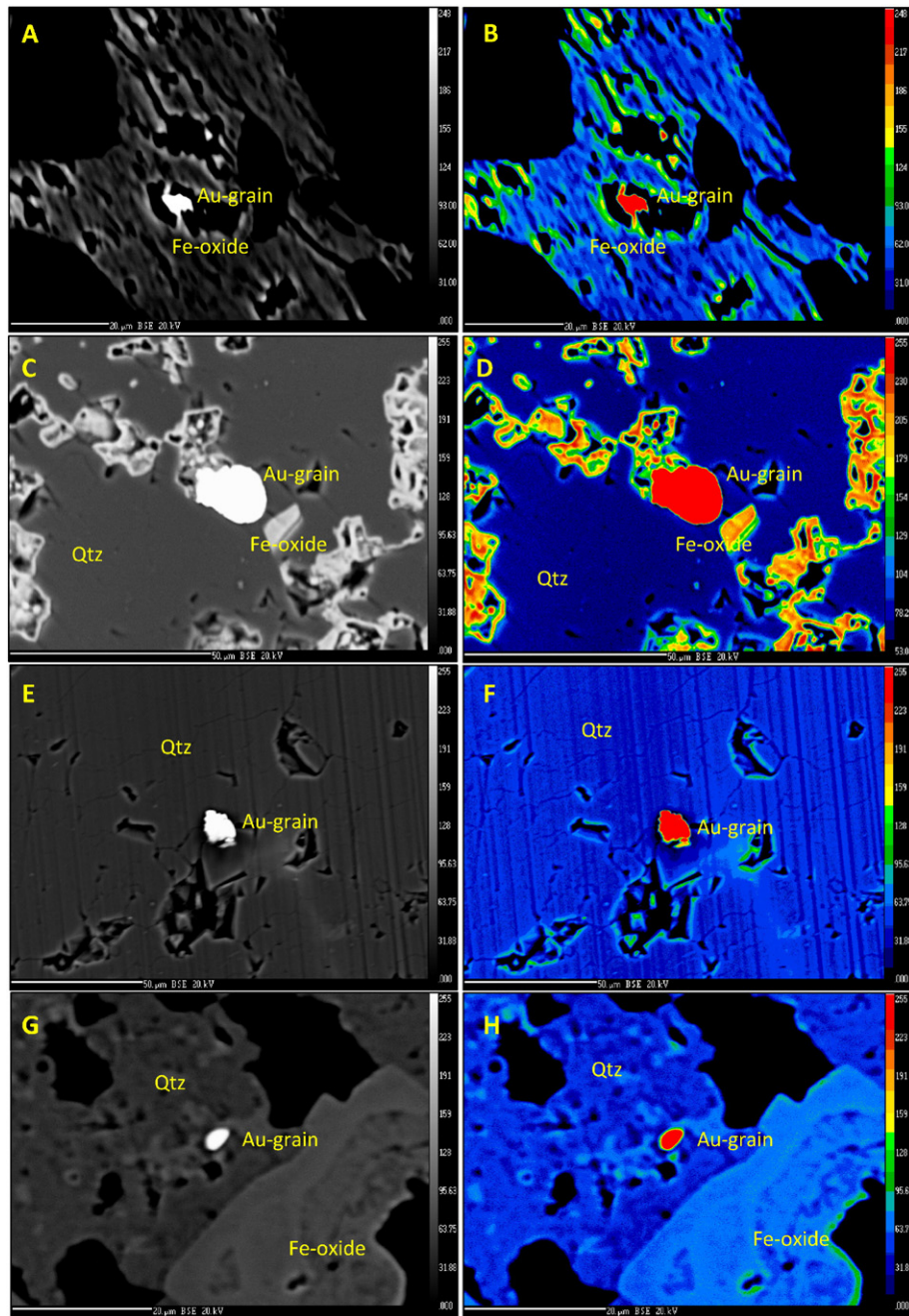


Fig. 3. Back scattered electron (BSE) images showing (A) and (B) occurrences of Au grains hosted in Fe-oxides of Ganajur BIF. (C) and (D) occurrences of Au grains in quartz veins cutting across Kudrekonda metavolcanic rocks. (E) and (F) Au–Ag alloy in BIF sample from Karajgi. (G) and (H) gold grain occurring in association with quartz and Fe-oxides in BIF from Karajgi.

the Kudrekonda samples (KK). The studied rocks exhibit maximum abundance of Sb which is considered as one of the path finder elements indicating presence of Au.

5.2. Geochemistry of BIF

BIF samples from Ganajur, Karajgi and Palavanahalli areas of Shimoga greenstone belt are characterized by variable SiO₂ (27.5–68.2 wt.%) and Fe₂O₃ (30.99–65.7 wt.%; Table 5) contents. Extremely high silica (78.43–97.1 wt.%) with much less iron (1.35–12.94 wt.%) concentrations in few samples classify them as cherty banded iron formations. Major element compositions of two BIF samples from Palavanahalli (P1 and P3) are overprinted by geochemical signatures of basic volcanic rocks owing to their close association. P2 is a ferruginous chert having high

concentrations of SiO₂ with low Fe₂O₃. ΣREE of the studied samples exhibits a wide variation from 9.3 to 102.1 ppm with Y abundances varying between 0.8 and 23 ppm. Majority of the BIF samples show high Y/Ho ratios ranging from 34 to 52.8, while few samples have lower values varying between 25 and 30 ppm. Most of the samples show superchondritic Y/Ho ratios (Y/Ho = 28.7–38.3). Post-Archean Australian Shale (PAAS) normalized REE patterns depict positive Eu and Tm anomalies with negative Ce and Yb anomalies (Fig. 8A, C, E and G). Chondrite normalized REE patterns reflect LREE enrichment over HREE and prominent LREE/HREE fractionation (Fig. 8 B, D, F and H). Among transitional trace elements, the BIF samples show low Ni, Cr, Co and Sc concentrations with variable enrichment in Vanadium. The large ion lithophile element (LILE) compositions are marked by low Rb and Cs contents and elevated Sr and Ba concentrations (Table 5).

Table 3

EPMA analyses of base metal sulphide associated with gold grains from BIFs and boninites of Shimoga greenstone belt.

wt.%	L-1		L-1		L-1		KK-8			L-1		KK-8		
	1	2	1	2	1	2	1	2	3	1	2	1	2	3
S	33.53	35.79	19.93	18.03	34.68	32.21	33.19	36.2	39.12	52.83	40.11	52.03	54.03	
Fe	29.27	24.79	33.33	37.66	9.43	7.58	8.95	6.77	10.55	45.3	58.4	44.79	45.35	
Co	0.05	0.01	–	0.03	0.05	–	0.01	–	0.03	0.05	0.02	0.16	0.02	
Ni	0.01	0.03	–	0.02	–	–	0.01	–	0.01	0.17	0.05	0.24	0.38	
Zn	0.03	–	0.09	–	53.11	58.48	56.11	54.01	49.94	0.03	0.09	–	0.02	
Ag	–	–	–	–	–	–	–	–	–	–	–	–	–	
Au	–	–	–	–	–	–	–	–	–	–	–	–	–	
Cu	35.62	38.03	0.03	0.06	–	–	0.2	0.17	0.08	0.01	0.06	0.03	0.02	
As	–	–	48.51	43.04	0.02	0.01	–	–	–	–	–	–	–	
Total	98.51	98.65	101.89	98.84	97.29	98.28	98.47	97.15	99.73	98.39	98.73	97.25	99.82	
Mineral	Chalcopyrite		Arsenopyrite		Sphalerite			Pyrite			Sphalerite			

M1: Ganajur BIF.

N11 and N5: Karajgi BIF.

KK8: Kudrekonda boninite.

High field strength element (HFSE) contents are low in these samples excepting relatively higher concentrations of Zr and Y (Table 5). The studied BIF samples show marked enrichment in Ag (630–2435 ppb) and Au

(706–15,831 ppb) with higher abundances of Au in comparison with Ag (Table 5). Relative abundances of Au, As and Sb in the BIF samples of Ganajur (L, M), Karajgi (N) and Palavanahalli (P) are depicted in Fig. 7.

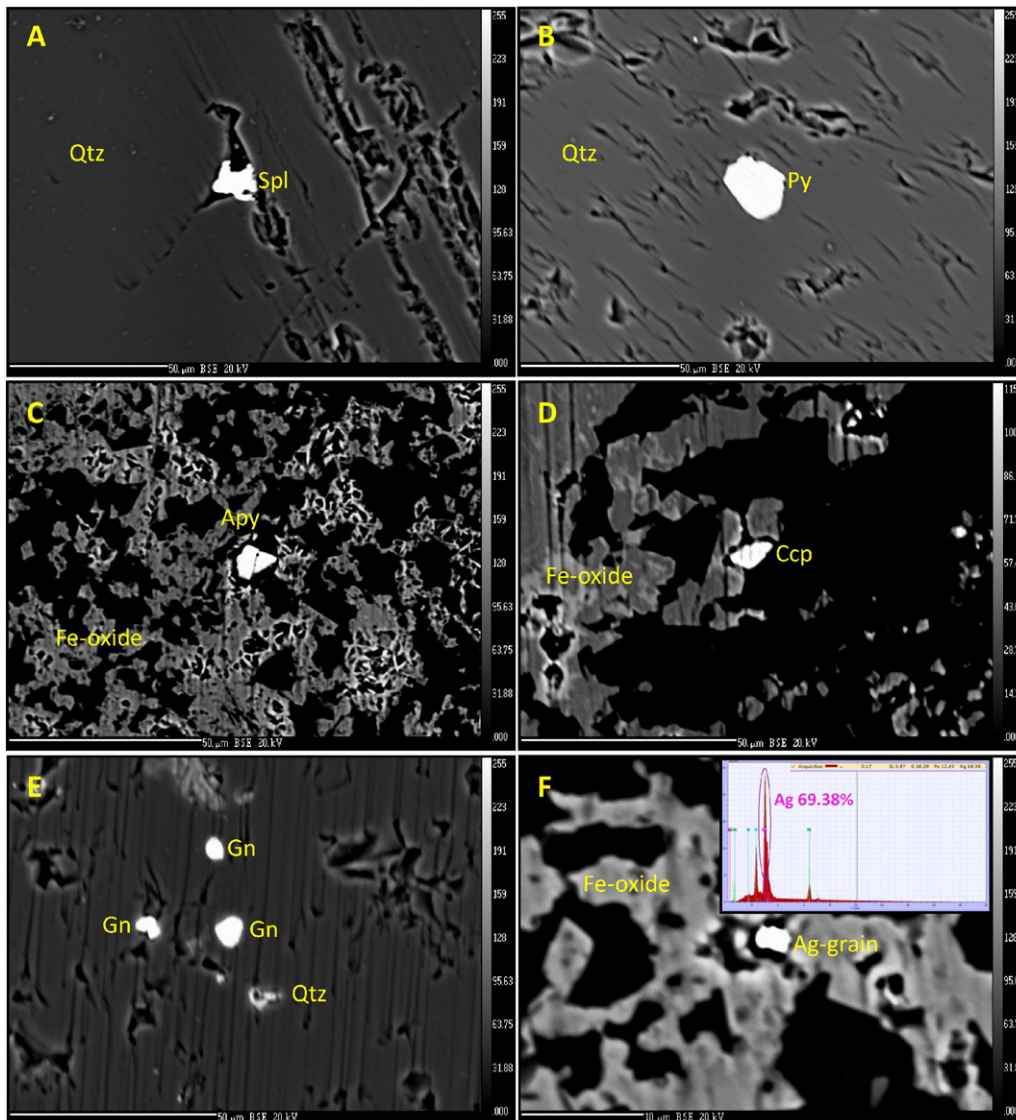


Fig. 4. Back scattered electron (BSE) images showing occurrences of (A) sphalerite and (B) pyrite in auriferous quartz veins. (C) Arsenopyrite (D) chalcopyrite and (E) galena occurring as sulphide phases in BIF; (F) Ag grain within Fe-oxides of BIF.

Table 4

Major, trace element and gold concentrations of Kudrekonda boninites.

wt.%	KK1	KK2	KK3	KK4	KK5	KK6	KK7	KK10	KK11	KK12	KK13	KK14
SiO ₂	45.16	37.9	37.67	36.44	43.84	39.94	44.89	35.75	41.41	35.64	33.7	26.4
TiO ₂	0.58	0.45	0.47	0.37	0.08	0.47	0.44	0.75	0.37	0.31	0.63	0.16
Al ₂ O ₃	13.68	12.57	11.86	11.69	6.04	13.47	11.29	10.11	12.83	11.62	18.02	8.76
Fe ₂ O ₃	9.97	11.26	7.61	7.59	5.27	9.67	9.57	9.03	9.54	9.23	10.93	6.48
MnO	0.07	0.14	0.1	0.14	0.15	0.11	0.08	0.23	0.1	0.14	0.1	0.2
MgO	25.37	26.18	27.22	27.58	22.09	24.47	27.64	25.94	25	27.04	22.66	30.52
CaO	0.21	5.02	7.8	10.05	18.84	2.02	0.36	13.48	3.2	9.66	2.24	24.02
Na ₂ O	0.05	0.08	0.37	2.25	0.5	2.42	0.03	2.12	0.99	0.25	0.09	0.29
K ₂ O	0.03	0.02	3.68	0.03	0.07	0.02	0.01	0.06	0.44	0.25	4.33	0.17
P ₂ O ₅	0.08	0.04	0.1	0.05	0.05	0.04	0.08	0.11	0.05	0.03	0.02	0.02
LOI	4.45	7.21	3.59	4.12	3.87	6.06	4.43	3.05	5.02	6.79	6.41	3.53
Total	99.65	100.87	100.47	100.31	100.8	98.69	98.82	100.63	98.95	100.96	99.13	100.55
Mg#	74	72	80	80	82	74	76	76	74	77	70	84
ppm												
Cr	521	3033	369	2660	584	3306	247	335	1546	2729	7966	1949
Co	87	96	43	66	69	93	61	66	55	86	116	74
Ni	626	591	193	705	193	669	279	203	492	716	1580	358
Rb	0.55	1.00	82.78	0.65	0.61	0.65	0.44	1.72	2.51	6.15	112	11.26
Sr	3.59	33.10	56.12	61	83	20.53	3.49	83	176	60.80	26.49	18.46
Cs	0.04	0.14	0.98	0.07	0.05	0.05	0.02	0.18	0.11	0.22	1.91	0.25
Ba	26.25	12.28	162	26.53	14.31	23.83	9.04	18.19	8.79	27.38	261	67
Sc	36	58	53	56	23	64	35	51	38	55	77	59
V	208	291	274	207	88	296	289	446	298	254	434	244
Nb	0.39	0.16	0.26	0.17	0.06	0.21	0.20	0.28	0.05	0.14	0.39	0.17
Ta	0.08	0.04	0.04	0.04	0.05	0.06	0.04	0.05	0.03	0.04	0.06	0.03
Zr	16.98	8.57	11.16	6.80	1.62	7.63	7.87	15.41	4.15	7.09	14.32	6.03
Hf	0.43	0.23	0.29	0.18	0.04	0.20	0.20	0.41	0.10	0.19	0.38	0.16
Th	0.29	0.11	0.20	0.13	0.06	0.15	0.13	0.09	0.05	0.19	0.21	0.11
U	0.24	0.69	0.12	0.21	0.14	0.17	0.08	0.02	0.09	0.08	0.11	0.17
Y	6.09	6.32	6.24	5.05	4.66	8.42	8.51	14.82	10.79	5.51	2.42	6.82
La	2.23	1.89	4.79	2.17	0.82	2.06	2.05	2.41	1.10	1.58	0.52	1.97
Ce	4.82	4.07	10.73	4.81	1.78	4.65	4.19	6.49	2.48	3.55	1.20	4.54
Pr	0.69	0.58	1.52	0.71	0.30	0.67	0.66	1.13	0.39	0.52	0.18	0.68
Nd	2.86	2.39	6.33	3.06	1.20	2.86	2.75	5.64	1.84	2.30	0.77	2.97
Sm	0.77	0.66	1.57	0.86	0.43	0.77	0.72	2.05	0.69	0.67	0.23	0.77
Eu	0.26	0.20	0.49	0.27	0.21	0.24	0.25	0.78	0.40	0.22	0.12	0.19
Gd	0.87	0.79	1.47	0.87	0.63	0.90	0.98	2.51	1.19	0.75	0.28	0.88
Tb	0.16	0.15	0.22	0.15	0.12	0.18	0.20	0.47	0.25	0.14	0.05	0.16
Dy	1.03	0.99	1.21	0.87	0.76	1.28	1.39	2.85	1.74	0.90	0.36	1.09
Ho	0.22	0.24	0.25	0.19	0.17	0.32	0.31	0.59	0.41	0.21	0.09	0.26
Er	0.74	0.82	0.84	0.70	0.61	1.09	1.03	1.83	1.39	0.73	0.39	0.91
Tm	0.12	0.14	0.14	0.13	0.11	0.19	0.16	0.29	0.23	0.13	0.08	0.15
Yb	0.84	0.95	1.00	0.95	0.80	1.20	0.97	1.85	1.50	0.91	0.62	1.00
Lu	0.15	0.17	0.18	0.18	0.15	0.20	0.15	0.30	0.25	0.17	0.11	0.17
Cu	35	47	181	31	30	29	41	64	87	36	32	31
Zn	83	144	62	89	45	111	54	135	89	79	94	74
Ga	13.50	13.55	17.48	10.51	4.07	14.18	15.01	22.97	12.73	11.49	25.70	12.13
Pb	9.94	16.70	14.23	13.98	11.12	14.10	11.58	103	15.02	12.78	12.82	10.55
As	38.46	32.50	38.04	30.14	27.69	29.43	32.91	33.23	18.22	33.70	34.36	30.88
Sb	2.71	1.88	1.99	2.44	0.69	2.81	2.65	0.64	0.48	1.59	3.15	1.64
ppb												
Ag	1881.60	2186.38	1795.05	2177.26	1733.96	2037.63	529.12	139.46	1184.12	949.33	1225.52	1251.27
Au	628.76	440.93	684.39	590.85	588.47	422.73	4.08	6.63	616.05	534.18	404.72	654.91
Al ₂ O ₃ /TiO ₂	23.59	27.93	25.23	31.59	75.50	28.66	25.66	13.48	34.68	37.48	28.60	54.75
CaO/Al ₂ O ₃	0.02	0.40	0.66	0.86	3.12	0.15	0.03	1.33	0.25	0.83	0.12	2.74
CaO/TiO ₂	0.36	11.16	16.60	27.16	236	4.30	0.82	17.97	8.65	31.16	3.56	150
Zr/Hf	39.45	37.32	38.63	37.36	38.88	37.42	38.56	37.25	40.14	37.77	37.55	38.39
Zr/Nb	43.23	55.24	42.82	41.16	28.25	35.94	39.11	54.54	82.36	48.93	36.56	35.59
Nb/Th	1.36	1.35	1.32	1.27	1.02	1.39	1.56	3.22	0.96	0.78	1.86	1.49
Th/Nb	0.74	0.74	0.76	0.78	0.98	0.72	0.64	0.31	1.04	1.29	0.54	0.67
Th/Ce	0.06	0.03	0.02	0.03	0.03	0.03	0.03	0.01	0.02	0.05	0.18	0.03
Gd/Yb	1.04	0.83	1.46	0.92	0.79	0.75	1.00	1.36	0.79	0.82	0.46	0.88
Dy/Yb	1.23	1.04	1.21	0.92	0.95	1.07	1.43	1.55	1.16	0.99	0.59	1.09
Nb/Nb*	0.03	0.02	0.01	0.01	0.05	0.03	0.02	0.02	0.02	0.02	0.10	0.01
Zr/Zr*	0.79	0.47	0.25	0.29	0.16	0.35	0.39	0.31	0.25	0.40	2.38	0.28
Hf/Hf*	0.73	0.46	0.23	0.28	0.14	0.34	0.37	0.31	0.23	0.38	2.29	0.26
Ti/Ti*	1.68	1.48	0.73	1.01	0.36	1.33	1.25	0.79	0.97	1.04	5.92	0.46
(La/Yb) _N	1.91	1.42	3.42	1.64	0.74	1.22	1.51	0.94	0.52	1.24	0.61	1.41
(La/Sm) _N	1.87	1.84	1.97	1.62	1.23	1.72	1.85	0.76	1.02	1.53	1.49	1.65
(Gd/Yb) _N	0.86	0.69	1.21	0.76	0.66	0.62	0.83	1.12	0.65	0.68	0.38	0.73
(Nb/La) _{PM}	0.17	0.08	0.05	0.07	0.07	0.10	0.09	0.11	0.04	0.09	0.72	0.08
(Th/La) _{PM}	1.05	0.49	0.33	0.48	0.55	0.60	0.51	0.29	0.39	0.96	3.26	0.47

Normalization factors after Sun and McDonough (1989).

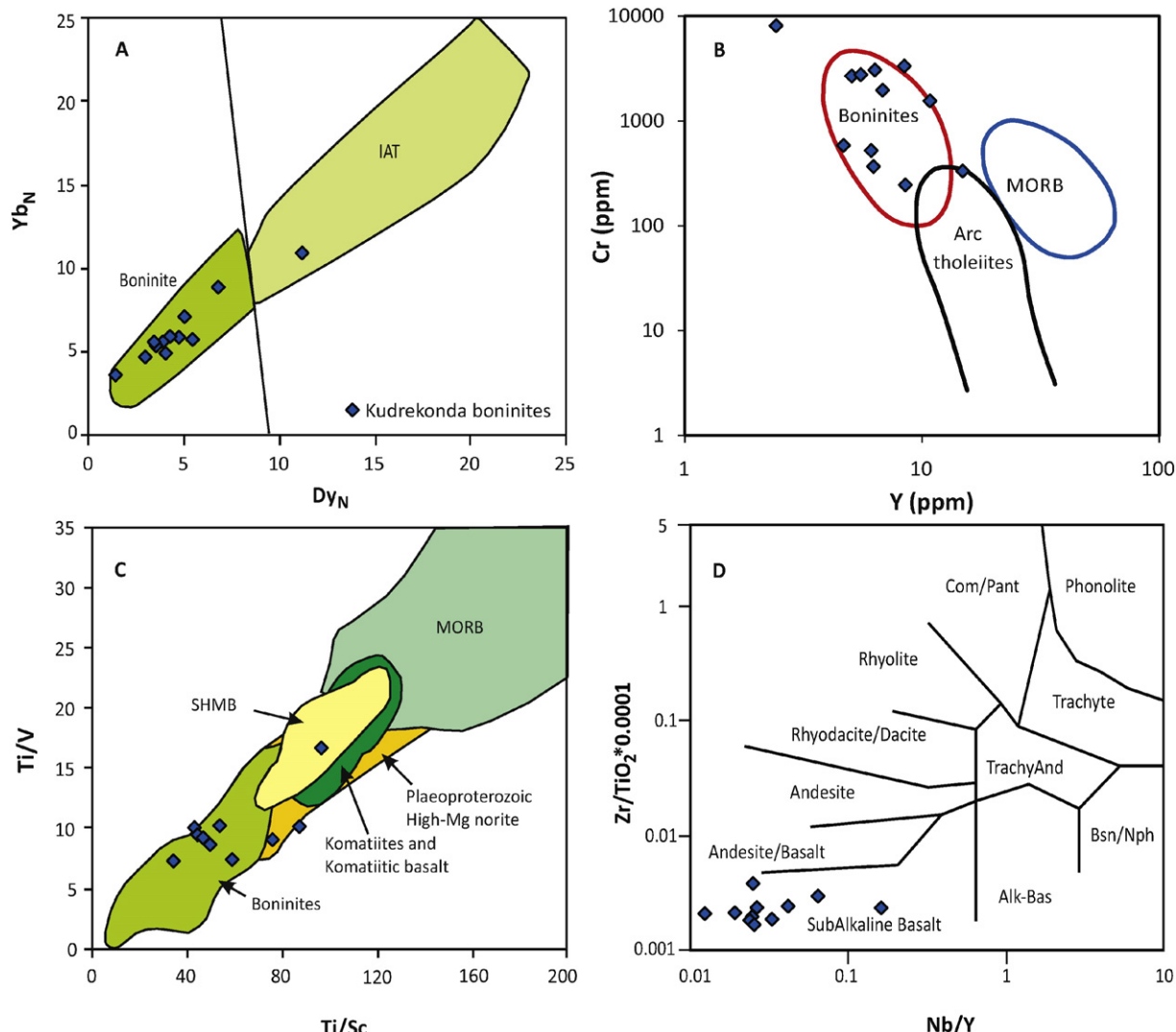


Fig. 5. (A) Yb_N vs. Dy_N plot (Dilek and Furnes, 2009) showing distinct fields for boninites and island arc tholeiites (IAT) where most of the studied metavolcanic rocks of Kudrekonda cluster in the boninite field. (B) Cr vs. Y discrimination figure (after Dilek et al. (2007)) classifying the studied samples as boninites. (C) Ti/Sc vs Ti/V diagram for Kudrekonda boninites. Majority of the studied metavolcanic samples occupy the fields of boninites. Fields of boninites, SHMB, komatiites, komatiitic basalts, High Mg norites are from Poidevin (1994), Smithies (2002) and Polat et al. (2002). (D) B) Nb/Y vs. $\text{Zr}/\text{TiO}_2 \times 0.0001$ diagram (after Winchester and Floyd (1977)) in which majority of the boninite samples fall in the field of sub-alkaline basalt.

The studied samples are characterized by maximum concentration of arsenic.

6. Discussion

6.1. Kudrekonda boninite: oceanic crust preserved in an active continental margin

The Kudrekonda mafic volcanic rocks of Shimoga greenstone belt characterized by >8 wt.% MgO , >40 wt.% SiO_2 and less than 0.5 wt.% TiO_2 are classified as boninites as per IUGS system (Crawford et al., 1981; 1989; Falloon et al., 1987; 2008; Pearce et al., 1992; Le Bas, 2000; Rubin et al., 2009; Xia et al., 2012). Phanerozoic boninites are primarily classified based on compositions of major oxides like SiO_2 , MgO , CaO , Al_2O_3 and TiO_2 (Crawford, 1989). However, in a strict sense, the high Mg volcanic rocks from Kudrekonda may be designated as "boninitic" or "boninite series", considering the mobility of these major elements (Si, Ca, Al) during seafloor hydrothermal alteration and metamorphism in Archean. In terms of immobile elements that remain unaffected by alteration and metamorphism, the geochemical signatures of the studied rocks are marked by i) high $\text{Al}_2\text{O}_3/\text{TiO}_2$ ratios of 30–60; (ii) U-shaped REE patterns with $(\text{La}/\text{Sm})_N > 1$ but $(\text{Gd}/\text{Yb})_N < 1$;

(iii) negative Nb anomalies where Nb/La is less than the primitive mantle value of 1.03 and (iv) high Mg#, Cr, Co, Ni contents relative to island arc tholeiites (IAT). These geochemical attributes are also in compliance with the Phanerozoic boninites (Sun and Mc Donough, 1989; Kerrich et al., 1998; Smithies, et al. 2004; Manikyamba et al., 2005). The elevated $\text{Al}_2\text{O}_3/\text{TiO}_2$, low TiO_2 of the Kudrekonda boninites in conjunction with U-shaped REE profile, $(\text{La}/\text{Sm})_N > 1$ and $(\text{Gd}/\text{Yb})_N < 1$ distinguish them from low-Ti tholeites ($\text{La}/\text{Sm}_N < 1$), siliceous high-Mg basalts (SHMB), Al-undepleted ($\text{Al}_2\text{O}_3/\text{TiO}_2 \leq 20$, flat HREE) and Al-depleted komatiites ($\text{Al}_2\text{O}_3/\text{TiO}_2 \leq 20$, $\text{Gd}/\text{Yb}_N > 1$; Sproule et al., 2002; Arndt, 2008; Stiegler et al., 2012).

In general, boninites occur in a variety of tectonic settings, including forearc regions of intraoceanic island arcs (Falloon and Crawford, 1991; Pearce et al., 1992), Phanerozoic and Proterozoic supra-subduction zone (SSZ) ophiolites (Rogers et al., 1989; Meffre et al., 1996; Wyman, 1999) and Archean greenstone belts (Kerrich et al., 1998) having a common association with intraoceanic subduction realms far away from continental crust (Piercey et al., 2001). The Bonin island of Izu-Bonin-Mariana intraoceanic arc system preserves the best exposure of boninites in the world that erupted on the sea floor around 46–48 Ma subsequent to the initiation of subduction at 52 Ma (Ishizuka et al., 2006, 2011; Stern et al., 2012). The 4.4–3.8 Ga Nuvvuagittuq supracrustal belt in Quebec,

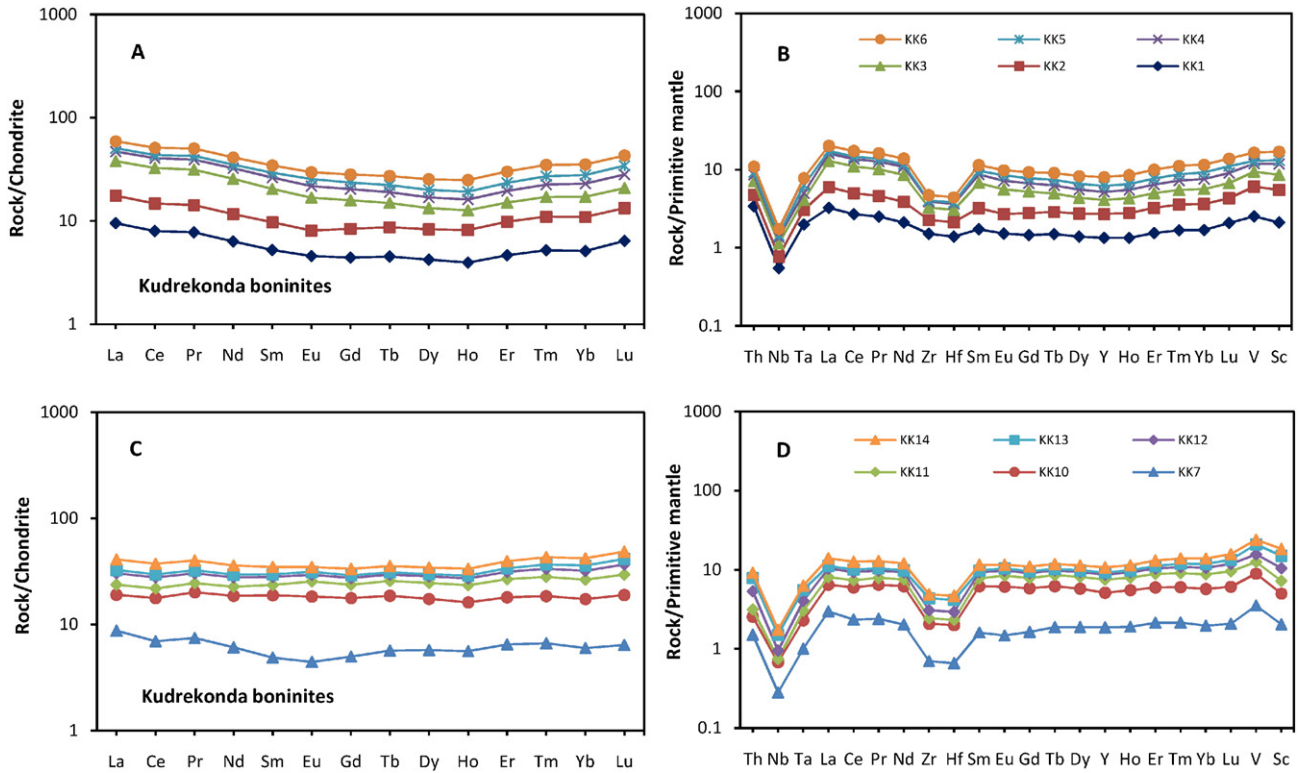


Fig. 6. (A) Chondrite normalized REE patterns for Kudrekonda boninites. (B) Primitive mantle normalized trace element patterns for Kudrekonda boninites. Normalizing factors are from Sun and Mc Donough (1989).

Canada and 3.7–3.8 Ga Isua greenstone belt of west Greenland preserve earliest evidence of boninite like volcanic rocks (Polat et al., 2002; Turner et al., 2014). Boninitic signatures from Archean greenstone terranes and their compositions analogous to the compositions of volcanic rocks of Phanerozoic Izu-Bonin-Mariana forearc imply that modern-style subduction processes were operative on earth dating back to the Hadean or Eoarchean (O'Neill et al., 2011, 2012; Turner et al., 2014). It has been envisaged that most Archean and Phanerozoic boninites are tectonically affiliated to ancient and modern intraoceanic arc systems respectively. However, boninites are extremely rare in active continental margins, with very few reported occurrences including boninitic volcanic rocks of Finlayson Lake region in southeastern Yukon, Canada, which erupted in a mid-Paleozoic continental margin arc- back arc setting (Piercey et al., 2001). The emplacement of Finlayson Lake boninites in an unusual active continental arc tectonic environment has been explained by propagation and accretion of a spreading ridge into an arc composed of oceanic and continental crust. The boninites erupted on the oceanic crust through asthenospheric upwelling that triggered partial melting of a refractory mantle wedge metasomatized by subduction-derived components. The felsic volcanic rocks contemporaneous with the boninites generated through intracrustal melting induced by upwelling asthenosphere in a continental arc regime (Piercey et al., 2001).

The Kudrekonda boninites exhibit prominent negative anomalies at Nb, Ta, Zr, Hf and Ti on primitive mantle normalised trace element patterns (Fig. 6B). These HFSE anomalies with $Nb/Nb^* = 0.02\text{--}0.46$ (with one exception of 1.01), $Zr/Zr^* = 0.17\text{--}0.69$, $Hf/Hf^* = 0.08\text{--}0.38$ (with one exception of 1.04) and $Ti/Ti^* = 0.71\text{--}1.27$ suggest significant LILE enrichment and relative HFSE depletion in the mantle which is attributed to release of fluid mobile large ion lithophile element (LILE) and light rare earth elements (LREE) into the mantle wedge by the influx of fluids dehydrated from the subducted oceanic slab. The infiltration of subduction derived fluids and their interaction with the depleted mantle wedge result into mantle wedge metasomatism and induce hydrous melting. However, the high field strength elements (HFSE) due to

their fluid immobile nature are retained in the dehydrated slab in a subduction regime (Gill, 1981; Perfit et al., 1980; Stern et al., 1991; Pearce et al., 1992; Konig et al., 2010). On Nb/Zr vs. Th/Zr plot, the Kudrekonda boninites exhibit a trend consistent with fluid related enrichment of mantle during the subduction process (Fig. 9A). The negative Zr anomalies in the studied samples attest to fractionation of Zr by amphibole that remained as a residual phase in the mantle. Most of the studied samples of boninites ($Zr/Nb: 28.2\text{--}82.4$; $Nb/Th: 0.8\text{--}3.2$) occupy the field of “arc” in Zr/Nb vs Nb/Th diagram (Figure not shown) suggesting their generation in an intraoceanic island arc environment. Th/Yb and Nb/Yb ratios are important proxies to constrain the nature of the mantle source that produce the parental magmas for these boninites upon partial melting. Variations of Th/Yb with respect to Nb/Yb (Fig. 9B), corroborate an intraoceanic island arc domain for the studied boninites and exhibit a distinct tholeiitic lineage for them. The boninite samples show depleted values of Nb/La and Th/La ratios ($Nb/La_{pm}: 0.04\text{--}0.7$, $Th/La_{pm}: 0.3\text{--}3.3$) with respect to primitive mantle and this feature is indicative of preferential retention of fluid immobile HFSE like Nb and Th in the subducted oceanic slab during slab dehydration and LREE enrichment of mantle wedge over HFSE. Chondrite-normalized REE patterns for Kundrekonda samples (Fig. 8A) exhibit typical MREE depletion relative to LREE and HREE abundances which conform to the characteristic REE signatures of boninites. The MREE show a compatible behaviour with amphibole which, with high partition coefficients for MREE relative to LREE and HREE, retains the MREE and remain as a residual phase in the source. Th/Ce ratio of Kudrekonda boninites (0.01–0.2) are higher than that of MORB ($Th/Ce = 0.016$) and OIB ($Th/Ce = 0.052$) attesting to negligible contribution from subducted pelagic sediments (Hawkesworth et al., 1997). However, the studied samples show lower Zr/Hf ratios (37.4–40.1) compared to the pelagic sediments ($Zr/Hf > 150$; Hole et al., 1984) discarding the possibility of pelagic input in their genesis. Low Th contents and Th/Nb ratios of the studied boninites ($Th: 0.05\text{--}0.3 \text{ ppm}$; $Th/Nb: 0.3\text{--}1.3$) negate incorporation of recycled sediments in the source. Dy/Yb is considered as a suitable geochemical proxy for identifying the domain of

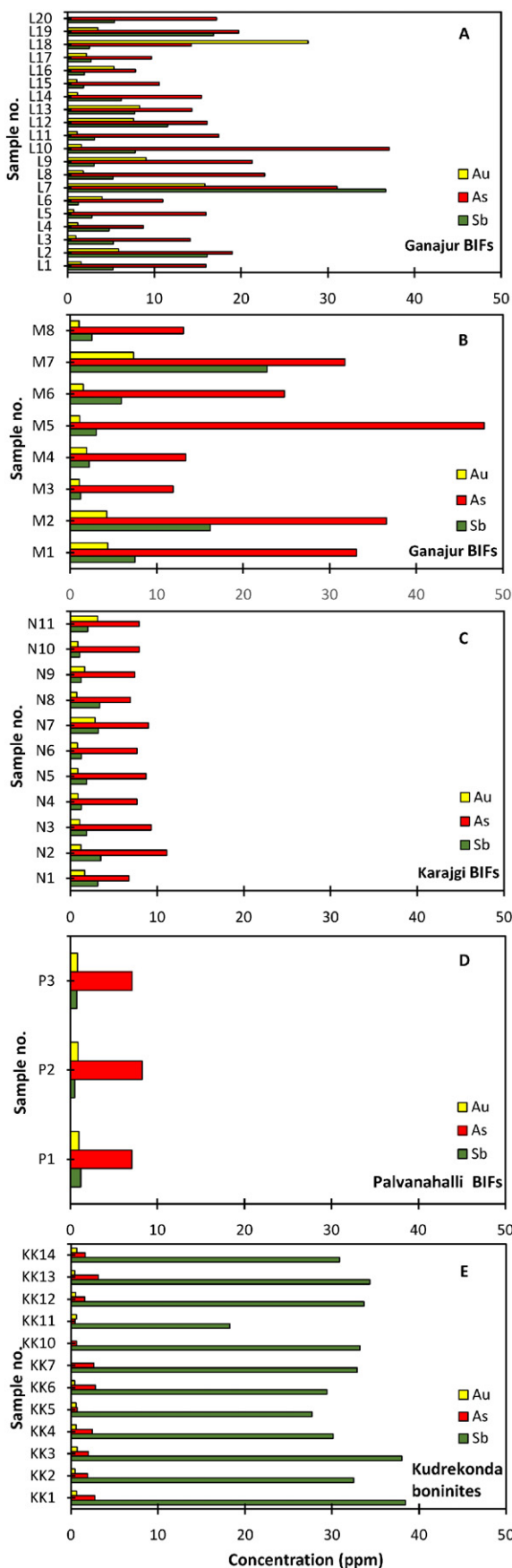


Fig. 7. Bar diagrams showing concentrations of gold (Au), arsenic (As) and antimony (Sb) in boninite samples from Kudrekonda (KK) and BIF samples from Ganajur (L,M), Karajgi (N) and Palvanahalli (P) areas of Shimoga greenstone belt.

partial melting with ratios <1.5 and >2.5 corresponding to the stability fields of amphibole/phlogopite-bearing spinel and garnet peridotite respectively (Yang et al., 2014). The Dy/Yb ratios for the Kudrekonda boninites (0.6–1.5) imply shallow level partial melting of a spinel peridotitic mantle and their negative Zr anomalies ($Zr/Zr^* = 0.17\text{--}0.69$) endorse residual amphibole in the mantle source. The Kudrekonda boninites occupy the field of spinel peridotite facies on Dy/Yb vs. La/Yb diagram (Fig. 9C) substantiate derivation of their parent melt in the stability field of spinel peridotite. The Gd/Yb ratios for these boninites, reaching a minimum value of 0.46, are lower than the modern depleted mantle (Gd/Yb: 0.98) thereby indicating the role of a depleted mantle residual from previous melt extraction events. This depleted refractory mantle was replenished in LILE and LREE through subduction-driven metasomatic enrichment that in turn accounts for the characteristic geochemical signatures of these boninites. These observations collectively infer hydrous melting of metasomatized mantle wedge of intraoceanic arc under high geothermal gradient and at shallow depth for the origin of Kudrekonda boninites.

In the Shimoga greenstone belt, the Kudrekonda boninites, occurring near the auriferous Honnali dome, correspond to the Kudrekonda Formation of the Bababudan Group. The felsic volcanic rocks of Shimoga greenstone belt occurring in Daginkatte and Shikaripura areas in the eastern and north-western parts of the Honnali dome correspond to the Daginkatte Formation of the lower Chitradurga Group that overlies the Bababudan Group in the stratigraphic sequence (Manikyamba et al., 2014a,b). The felsic volcanic rocks of Daginkatte Formation have been dated at 2614 ± 5 Ma by SHRIMP U–Pb dating thereby indicating a Neoarchean age of their eruption. However, geochronological data is not available on the mafic volcanic rocks of Kudrekonda till date. Therefore, based on the geological setting, stratigraphic succession and geochronological evidence (only for felsic volcanic rocks), it is considered that the generation of Kudrekonda boninites are older than the felsic volcanic rocks, preceded the eruption of Daginkatte rhyolites and these two lithotypes are not contemporaneous and correspond to different tectonic settings. The felsic volcanic rocks of Shimoga greenstone belt were generated in an active continental margin setting where partial melting of (i) mantle wedge carrying subduction inputs and (ii) lower continental crust with assimilation of upper crustal components collectively contributed to their continental arc signatures (Manikyamba et al., 2014b). In contrast to this, the Kudrekonda boninites show characteristic intraoceanic arc affinity augmenting the role of a depleted mantle wedge metasomatized by subduction-derived fluids that is concomitant with the initial stages of intraoceanic subduction. Therefore, both these lithotypes reflect subduction-derived geochemical features attributable to continental and oceanic arc magmatism. The boninites and felsic volcanic rocks (predominantly rhyolites) belong to different stratigraphic groups indicating their origin through distinct phases of subduction zone magmatism in diverse tectonic environments that collectively contributed towards the evolution of the Shimoga greenstone belt in western Dharwar Craton. However, in absence of consolidated geochronological data for Kudrekonda boninites, this issue emerges as an open forum for future investigations.

6.2. Hydrothermal signatures of Shimoga BIF

BIFs were formed during Archean and Paleoproterozoic timeframe with maximum abundance between 2700 and 2300 Ma that was concomitant with the ‘Great Oxidation Event’ heralding marked changes in the redox conditions of the paleoceans and atmosphere (Cloud, 1965; Kasting, 1993; Holland, 1973, 2006; Klein, 2005). Conventional models conform to BIF deposition through oxidation of Fe(II) in the presence of free oxygen derived from oxygenic microbial photosynthesis thereby attesting to the role of BIFs in rise of earth’s atmospheric oxygen, compositional change in hydrosphere and diversification of the biosphere (Cloud, 1965; Klein and Beukes, 1989; Morris, 1993; Konhauser et al., 2009). The relation between BIF formation and free

Table 5
Major, trace element and gold concentrations of Ganajur BIFs.

wt.%	L1	L2	L3	L4	L5	L6	L7	L8	L9	L10	L11	L12	L13	L14	L15	L16	L17	L18	L19	L20	M1
SiO ₂	29.89	40.31	53.22	50.72	34.27	34.17	42.82	33.2	34.46	30.5	58.52	84.12	62.99	51.99	33.35	27.48	58.63	27.93	52.59	41.57	34.7
TiO ₂	0.05	0.29	0.02	0.03	0.05	0.03	0.1	0.04	0.03	0.08	0.22	0.04	0.03	0.21	0.04	0.05	0.1	0.04	0.06	0.06	0.03
Al ₂ O ₃	1.27	4.83	0.9	0.5	1.78	0.82	2.8	1.12	1.29	3.06	4.86	0.92	0.76	4.31	0.92	1.02	2	0.86	1.42	1.7	0.57
Fe ₂ O ₃	62.29	46.76	41.63	45.12	60.24	60.2	47.6	60.41	59.7	60.67	31.01	12.94	31.07	38.17	60.01	65.67	35.65	65.34	41.53	51.62	59.88
MnO	0.03	0.06	0.02	0.01	0.04	0.02	0.04	0.02	0.03	0.15	0.24	0.02	0.02	0.04	0.06	0.05	0.06	0.06	0.02	0.04	0.03
MgO	0.33	0.18	0.54	0.09	0.09	0.12	0.14	0.16	0.12	0.17	0.16	0.01	0.08	0.16	0.09	0.08	0.13	0.06	0.08	0.2	0.08
CaO	0.19	0.19	0.2	0.14	0.16	0.18	0.19	0.18	0.2	0.33	0.22	0.15	0.15	0.38	0.17	0.24	0.28	0.17	0.15	0.27	0.22
Na ₂ O	0.09	0.33	0.03	0.04	0.23	0.1	0.29	0.07	0.1	0.36	0.72	0.24	0.07	0.62	0.08	0.13	0.2	0.08	0.17	0.14	0.05
K ₂ O	0.22	1.27	0.04	0.04	0.24	0.12	0.46	0.16	0.17	0.58	0.74	0.26	0.11	0.67	0.19	0.17	0.43	0.16	0.23	0.32	0.05
P ₂ O ₅	0.13	0.11	0.15	0.09	0.15	0.16	0.14	0.12	0.17	0.16	0.12	0.06	0.09	0.13	0.09	0.11	0.09	0.1	0.14	0.13	
LOI	5.17	4.43	2.66	2.68	3.67	4.81	4.53	4.22	3.71	4.15	2.89	1.1	2.88	3.12	4.54	4.58	3.04	4.36	3.18	3.6	3.9
Sum	99.66	98.76	99.41	99.46	100.92	100.73	99.11	99.7	99.98	100.21	99.7	99.86	98.25	99.8	99.54	99.56	100.63	99.15	99.53	99.66	99.64
ppm																					
Cr	12.60	14.26	16.09	13.16	10.76	11.84	13.10	12.06	10.61	11.41	15.11	18.51	15.72	14.70	12.60	10.53	16.64	11.51	14.84	12.98	12.02
Co	5.40	5.14	7.04	5.22	3.87	3.54	7.44	4.81	4.29	8.25	10.25	5.89	2.98	5.06	5.53	3.47	6.23	5.75	3.20	5.07	5.06
Ni	12.50	12.01	13.92	13.52	11.22	10.65	11.17	10.70	11.15	12.05	12.26	11.18	9.80	10.64	10.88	9.51	11.39	11.93	10.12	11.10	13.22
Rb	1.94	9.88	0.47	0.22	1.91	0.95	3.57	1.46	1.34	4.53	5.84	1.20	1.01	5.42	1.71	1.07	3.64	1.98	1.91	2.91	1.27
Sr	51	77	23	19	167	42	274	46	424	123	152	71	30	206	22	23	53	31	33	113	86
Cs	2.09	8.70	2.52	0.84	2.47	1.23	3.55	2.15	1.63	4.12	5.70	2.42	1.50	6.58	1.66	1.08	3.80	2.43	2.37	2.60	1.59
Ba	61	275	41	34	149	36	156	84	122	312	318	63	61	134	167	39	140	55	57	120	61
Sc	1.93	5.92	1.33	0.52	0.98	0.64	2.54	1.14	0.95	2.21	4.15	1.14	0.60	3.94	0.83	0.64	1.63	1.10	0.93	1.98	1.08
V	22	61	18.80	11.88	15.20	12.33	31	20	23	30	38	12.46	12.22	39	12.82	10.73	21	17.89	13.17	21	11.95
Nb	1.12	4.42	0.46	0.64	1.15	0.61	1.64	0.92	0.66	1.74	3.34	0.69	0.46	2.80	0.90	0.57	1.83	0.83	1.01	1.16	1.31
Ta	0.08	0.50	0.05	0.04	0.08	0.05	0.20	0.07	0.04	0.19	0.40	0.07	0.04	0.37	0.09	0.05	0.18	0.06	0.14	0.13	0.71
Zr	10.81	53	2.72	4.39	4.45	6.56	19.59	9.80	3.45	26	44	4.02	2.33	38	9.85	9.90	27	6.39	6.43	6.57	8.55
Hf	0.42	2.15	0.11	0.16	0.19	0.22	0.71	0.34	0.14	0.94	1.59	0.19	0.10	1.32	0.35	0.32	0.90	0.27	0.35	0.33	0.31
Th	0.89	3.16	0.21	0.23	0.54	0.34	1.40	1.39	0.38	1.19	3.25	0.59	0.22	2.48	0.64	0.40	1.21	0.47	0.73	0.98	0.45
U	0.50	0.71	0.36	0.14	0.60	0.33	1.17	1.21	0.33	0.80	0.72	0.57	0.57	1.22	0.39	0.46	0.52	1.10	0.53	0.58	0.98
Y	6.18	13.21	15.58	2.19	6.86	6.02	9.53	5.90	7.19	12.86	13.35	3.81	4.90	9.99	6.75	4.92	6.94	7.71	4.29	9.51	7.10
La	3.93	14.84	6.15	2.27	4.41	5.03	7.03	4.66	8.43	10.15	16.78	3.93	2.65	12.31	3.68	2.18	5.86	4.72	5.95	6.72	3.83
Ce	5.82	23.45	10.12	3.12	6.71	7.11	11.41	6.58	10.92	16.41	27.08	5.96	3.50	19.19	5.36	3.25	9.05	7.28	8.30	10.58	5.51
Pr	0.75	3.00	1.36	0.45	0.86	0.86	1.48	0.83	1.68	2.23	3.42	0.73	0.44	2.32	0.70	0.41	1.17	0.98	0.93	1.38	0.70
Nd	2.97	11.38	5.81	1.95	3.57	3.24	5.95	3.24	7.09	9.31	12.74	2.83	1.74	8.56	2.85	1.66	4.64	4.09	3.12	5.70	2.86
Sm	0.58	2.02	1.46	0.35	0.77	0.58	1.23	0.67	1.45	2.09	2.25	0.57	0.36	1.48	0.57	0.36	0.99	0.89	0.43	1.33	0.60
Eu	0.25	0.60	0.67	0.13	0.36	0.20	0.56	0.34	0.63	0.77	0.62	0.21	0.19	0.46	0.26	0.15	0.30	0.31	0.14	0.49	0.20
Gd	0.61	2.09	1.45	0.36	0.71	0.61	1.18	0.69	1.42	1.98	2.33	0.55	0.40	1.52	0.60	0.36	0.95	0.82	0.55	1.22	0.65
Tb	0.07	0.22	0.21	0.03	0.08	0.06	0.13	0.08	0.13	0.21	0.23	0.06	0.05	0.16	0.07	0.05	0.11	0.09	0.05	0.14	0.07
Dy	0.59	1.72	1.88	0.23	0.69	0.50	1.10	0.66	0.89	1.61	1.80	0.51	0.45	1.29	0.58	0.41	0.85	0.76	0.40	1.15	0.67
Ho	0.14	0.37	0.38	0.05	0.15	0.12	0.24	0.15	0.18	0.33	0.38	0.10	0.11	0.28	0.14	0.10	0.18	0.17	0.09	0.24	0.15
Er	0.36	0.96	0.89	0.13	0.38	0.31	0.62	0.39	0.48	0.85	1.03	0.26	0.28	0.75	0.38	0.27	0.49	0.45	0.27	0.61	0.42
Tm	0.08	0.20	0.17	0.03	0.08	0.06	0.12	0.09	0.09	0.16	0.21	0.05	0.06	0.16	0.08	0.06	0.10	0.10	0.06	0.12	0.09
Yb	0.44	1.15	0.83	0.14	0.45	0.36	0.71	0.50	0.54	0.92	1.19	0.31	0.33	0.93	0.49	0.35	0.58	0.55	0.33	0.72	0.53
Lu	0.08	0.20	0.12	0.03	0.08	0.07	0.12	0.09	0.09	0.15	0.20	0.05	0.06	0.16	0.09	0.06	0.10	0.10	0.06	0.13	0.10
Cu	52	43	34	33	41	26	160	35	45	69	44	36	31	60	33	29	47	39	29	48	91
Zn	199	105	104	101	94	80	107	91	126	127	102	111	113	108	79	80	87	145	68	78	264
Ga	3.37	14	3.84	2.65	3.93	1.78	7.91	2.62	2.59	6.73	9.08	3.88	1.50	9.21	2.05	1.30	4.00	2.59	3.58	4.38	2.89
Pb	32	65	16	22	19	18	73	18	18.9	36	15	18	21	22	15	15	21	30	36	36	56
As	15.95	18.98	14.15	8.73	15.94	10.98	31.07	22.71	21.28	37.12	17.43	16.10	14.35	15.45	10.57	7.83	9.67	14.25	19.74	17.18	33
Sb	5.24	16.10	5.25	4.78	2.79	1.23	36.70	5.23	3.06	7.80	3.10	11.52	7.74	6.18	1.83	1.92	2.70	2.50	16.83	5.39	7.49
ppb																					
Ag	1867.50	1720.25	2435.27	1564.90	1602.92	889.48	998.89	1105.26	1309.19	1349.91	1060.99	1795.75	1494.76	1437.91	1597.70	1541.41	1667.75	1771.42	1323.80	1990.22	1720.28
Au	1555.82	5865.51	944.98	1161.88	2076.14	706.00	3946.17	15831.73	1806.15	9052.16	1589.58	1096.20	7609.29	8298.02	1148.48	1070.15	5359.60	2162.25	27740.08	3491.66	4340.89
Th/U	1.78	4.43	0.58	1.58	0.91	1.02	1.19	1.15	1.16	1.48	4.53	1.04	0.39	2.03	1.64	0.88	2.33	0.43	1.37	1.67	0.46
Y/Ho	45.78	36.10	40.76	43.41	46.16	51.26	39.49	39.64	39.62	39.14	35.12	36.45	46.23	35.71	48.07	50.29	37.82	45.77	45.14	39.39	47.64
Σ REE	16.67	62.20	31.51	9.28	19.31	19.10															

Table 5 (continued)

wt.%	M2	M3	M4	M5	M6	M7	M8	N1	N2	N3	N4	N5	N6	N7	N8	N9	N10	N11	P1	P2	P3
SiO ₂	48.22	34.05	34.23	50.15	54.76	58.99	37.66	28.31	83.64	85.11	56.18	78.43	58.08	58.9	60.46	39.32	31.88	32.93	68.16	97.12	50.25
TiO ₂	0.14	0.02	0.04	0.38	0.05	0.05	0.02	0.03	0.08	0.04	0.38	0.34	0.12	0.13	0.04	0.04	0.04	0.06	0.02	0.06	1.25
Al ₂ O ₃	3.72	0.42	0.67	10.31	1.05	2.07	0.38	0.69	1.2	0.5	9.13	4.27	4.26	2.71	0.92	0.8	1.24	1.08	2.55	0.55	11.37
Fe ₂ O ₃	41.91	60.64	60.43	30.99	40.46	33.69	56.15	64.71	12.55	11.87	5.21	12.73	33.08	34.18	34.46	54.45	61.7	60.93	4.03	1.35	10.12
MnO	0.02	0.06	0.03	0.05	0.03	0.02	0.03	0.01	0.01	0.03	0.02	0.01	0.01	0.02	0.02	0.06	0.06	0.07	0.18	0.09	0.13
MgO	0.11	0.07	0.06	0.64	0.09	0.12	0.06	0.18	0.02	0.11	4.96	0.11	0.13	0.18	0.33	0.33	0.16	0.19	3.21	0.02	11.67
CaO	0.21	0.15	0.32	0.22	0.18	0.25	0.15	0.16	0.08	0.11	14.11	0.08	0.16	0.21	0.18	0.15	0.15	0.19	18.69	0.07	8.56
Na ₂ O	0.38	0.03	0.07	0.83	0.06	0.12	0.02	0.04	0.12	0.08	0.21	0.18	0.23	0.08	0.03	0.04	0.07	0.06	0.12	0.07	2.76
K ₂ O	0.7	0.06	0.11	2.62	0.23	0.26	0.05	0.15	0.55	0.4	3.38	1.59	1.09	0.39	0.12	0.18	0.34	0.28	0.07	0.46	0.49
P ₂ O ₅	0.14	0.12	0.21	0.07	0.11	0.16	0.12	0.15	0.12	0.1	0.04	0.05	0.11	0.09	0.09	0.1	0.13	0.14	0.03	0.03	0.12
LOI	3.53	3.57	3.71	3.91	3.65	2.97	4.6	5.72	1.71	1.57	6.57	2.38	3.52	2.82	3.29	4.96	4.73	4.79	3.01	0.23	4.1
Sum	99.08	99.19	99.88	100.17	100.67	98.7	99.24	100.15	100.08	99.92	100.19	100.17	100.79	99.71	99.94	100.43	100.5	100.72	100.07	100.05	100.82
ppm																					
Cr	15.77	11.76	11.71	15.01	16.81	17.70	12.92	13.15	21.56	17.74	14.40	15.70	14.10	14.34	12.21	10.61	13.34	13.15	30.09	26.87	20.82
Co	5.42	5.24	4.02	28.09	6.94	6.78	5.28	3.03	3.63	3.30	6.86	5.25	4.38	2.84	5.96	5.39	4.80	4.35	13.48	4.02	5.67
Ni	13.55	12.39	10.84	19.37	12.69	13.39	12.54	11.74	14.66	12.79	21.73	12.94	13.80	11.93	12.84	12.50	12.75	11.26	17.53	10.07	11.27
Rb	7.17	0.92	1.26	24	2.52	2.56	0.61	1.65	3.49	2.39	22	14.59	11.12	4.36	1.39	2.01	3.51	3.01	0.20	0.18	2.05
Sr	189	23	41	114	47	94	36	15.39	28	27	126	36	34	27	12.17	24	22	21	129	9.78	11.81
Cs	6.17	1.06	1.77	17.84	3.04	3.35	1.10	1.82	2.79	2.09	21	21	10.72	8.27	1.88	1.58	2.36	2.46	0.54	0.46	0.96
Ba	174	34	66	473	111	138	38	50	141	90	411	509	453	179	48	88	138	95	29	73	90
Sc	3.50	0.73	1.03	10.27	1.45	2.76	1.08	1.12	1.95	0.63	8.40	5.80	3.64	1.51	0.95	0.72	1.15	1.11	4.81	0.21	0.96
V	41	5.88	9.43	91	15.06	26	10.96	11.33	32	13.78	91	56	36	23	9.48	8.59	18.13	15.66	30	9.08	23
Nb	2.70	0.60	1.62	8.44	1.13	1.02	0.58	158	1.93	1.28	9.55	5.16	3.40	2.96	1.67	0.72	0.86	1.32	0.28	0.17	0.70
Ta	0.40	0.11	0.58	1.07	0.28	0.15	0.17	13.77	0.26	0.12	1.17	0.64	0.42	0.23	0.38	0.13	0.07	0.13	0.02	0.01	0.07
Zr	42	7.54	12.97	97	15.99	11.96	5.83	6.28	11.52	8.15	89	55	31	23	7.57	7.18	7.06	10.52	0.86	0.43	1.51
Hf	1.57	0.31	0.56	4.59	0.73	0.55	0.29	0.29	0.54	0.29	3.40	2.13	1.14	0.84	0.29	0.28	0.25	0.38	0.04	0.02	0.08
Th	2.94	0.29	0.50	5.38	1.02	1.18	0.46	0.46	1.08	0.59	5.16	3.88	2.22	1.48	1.75	0.52	0.51	0.80	0.11	0.05	0.17
U	1.17	0.60	0.21	1.39	1.04	1.29	0.53	0.30	0.47	1.02	0.99	1.06	0.66	0.44	0.52	0.48	0.46	0.53	0.53	0.29	0.16
Y	8.13	7.48	5.51	23.01	5.40	9.39	6.47	8.13	6.91	4.79	15.13	13.74	12.60	7.99	6.63	6.38	7.92	7.10	4.72	0.81	2.51
La	14.82	2.62	3.38	22.57	6.10	8.01	3.60	4.36	5.72	4.34	21.34	19.42	11.87	6.10	4.61	3.34	5.75	4.76	1.92	0.77	2.85
Ce	23.18	3.54	5.37	37.11	9.55	12.67	5.31	6.67	8.14	6.10	36.73	30.28	18.31	9.12	6.95	4.74	8.36	7.24	3.39	1.42	4.65
Pr	2.89	0.45	0.68	4.76	1.26	1.72	0.71	0.87	1.18	0.85	4.51	3.72	2.41	1.10	0.88	0.67	1.14	0.97	0.49	0.17	0.71
Nd	11.07	1.94	2.70	18.69	4.97	6.96	3.04	3.61	4.67	3.29	17.48	13.64	9.54	3.95	3.37	2.91	4.85	4.02	2.21	0.68	3.17
Sm	2.04	0.44	0.52	4.07	0.98	1.47	0.67	0.75	0.92	0.68	3.61	2.19	1.88	0.67	0.69	0.70	1.04	0.84	0.62	0.16	0.84
Eu	0.56	0.19	0.20	1.00	0.35	0.48	0.24	0.30	0.34	0.24	0.85	0.63	0.62	0.33	0.29	0.35	0.54	0.45	0.27	0.06	0.28
Gd	1.97	0.46	0.54	4.16	1.05	1.48	0.67	0.79	0.95	0.68	3.53	2.43	1.94	0.81	0.74	0.71	1.08	0.88	0.61	0.16	0.71
Tb	0.17	0.06	0.06	0.47	0.09	0.15	0.08	0.09	0.10	0.07	0.35	0.23	0.20	0.09	0.08	0.08	0.11	0.09	0.08	0.02	0.08
Dy	1.12	0.57	0.51	3.71	0.66	1.20	0.62	0.73	0.79	0.55	2.66	1.84	1.65	0.84	0.65	0.64	0.85	0.74	0.72	0.16	0.56
Ho	0.23	0.14	0.12	0.74	0.14	0.25	0.14	0.17	0.17	0.11	0.52	0.40	0.37	0.19	0.15	0.14	0.18	0.16	0.16	0.03	0.10
Er	0.63	0.40	0.32	1.91	0.37	0.67	0.39	0.48	0.45	0.29	1.37	1.11	0.94	0.53	0.40	0.38	0.50	0.42	0.44	0.07	0.23
Tm	0.13	0.09	0.07	0.39	0.07	0.13	0.08	0.11	0.09	0.05	0.28	0.23	0.19	0.11	0.08	0.08	0.10	0.09	0.10	0.01	0.04
Yb	0.79	0.53	0.40	2.20	0.44	0.78	0.46	0.62	0.54	0.29	1.68	1.36	1.12	0.62	0.46	0.47	0.60	0.54	0.63	0.07	0.25
Lu	0.15	0.09	0.07	0.35	0.08	0.13	0.09	0.12	0.10	0.05	0.28	0.23	0.18	0.10	0.08	0.09	0.11	0.10	0.12	0.01	0.04
Cu	106	93	73	99	79	106	87	73	80	89	80	87	75	84	78	70	90	108	29	33	43
Zn	232	205	243	198	254	285	186	176	164	199	408	213	272	163	220	214	253	234	108	46	233
Ga	10.88	1.86	2.94	24	5.44	7.48	2.08	3.53	5.40	3.34	16.76	8.08	7.40	9.39	1.96	2.29	5.21	4.70	1.24	0.36	2.79
Pb	75	38	111	35	45	340	92	38	75	56	52	30	23	183	40	24	107	74.02	12.48	20	13.54
As	37	11.91	13.34	47.85	24.75	31.77	13.09	6.76	11.14	9.33	7.69	8.75	7.69	9.03	6.94	7.44	7.96	7.94	7.06	7.95	8.23
Sb	16.19	1.20	2.18	3.01	5.93	22.74	2.51	3.18	3.52	1.91	1.27	1.90	1.28	3.24	3.41	1.25	1.10	2.01	1.17	0.52	0.48
ppb																					
Ag	1703.33	886.95	1674.86	1331.50	630.86	1069.39	1245.73	1397.12	655.75	1028.47	893.98	952.15	1339.26	1889.64	791.25	867.27	1006.56	850.55	1719.85	1403.58	1664.76
Au	4221.30	1080.12	1925.96	1103.91	1529.27	7324.86	1019.91	1672.03	1229.93	1091.00	905.83	877.62	810.34	2839.32	766.12	1640.20	869.08	3137.62	854.47	794.07	941.77
Th/U	2.51	0.49	2.43	3.86	0.98	0.91	0.87	1.51	2.28	0.58	5.21	3.67	3.37	3.40	3.36	1.08	1.12	1.51	0.20	0.17	1.09
Y/Ho	35.80	52.81	46.73	30.94	39.46	37.83	45.22	47.62	41.26	42.99	28.95	33.93	34.04	41.30	44.84	46.20	43.09	45.01	29.08	26.56	25.51
Σ REE	59.74	11.52	14.95	102.13	26.10	36.10	16.09	19.65	24.15	17.											

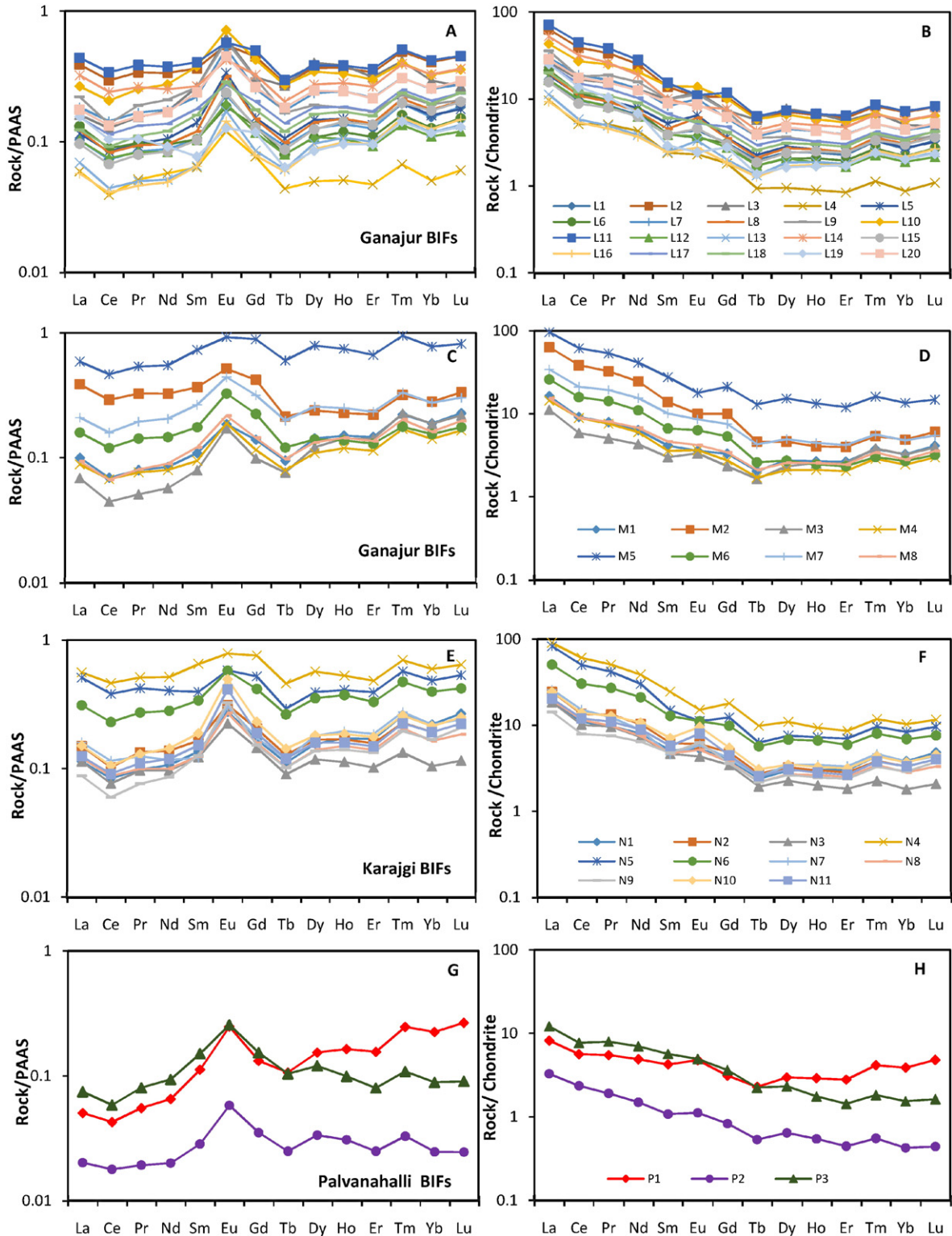


Fig. 8. (A, C, E and G) PAAS normalized and (B, D, F and G) Chondrite normalized REE patterns for BIF samples from Ganajur (L,M), Karajgi (N) and Palavanahalli (P) areas of Shimoga greenstone belt.

O_2 produced by photosynthetic microbes has been discarded by other models invoking oxidation of dissolved Fe(II) by anaerobic photosynthetic bacteria (Konhauser et al., 2002; Kappler et al., 2005; Posth et al., 2008; Pecoits et al., 2009). BIFs are classified into two types based on the sedimentary and tectonic environments for their deposition (Gross, 1996; Wang et al., 2014). The Algoma-type BIF is smaller in size and thickness, associated with mafic/ultramafic to felsic volcanic

rocks or volcaniclastic rocks and greywackes and deposited in arc/back-arc basins or intracratonic rift zones. The Superior-type BIF is thicker, occur in association with clastic-carbonate rocks and deposited in shallow marine conditions during transgressive phase, on the continental shelves of passive tectonic margins or in intracratonic basins. Transition type BIFs are characterized by a transitional depositional regime shifting between continental shelves and deep water regions (González et al.,

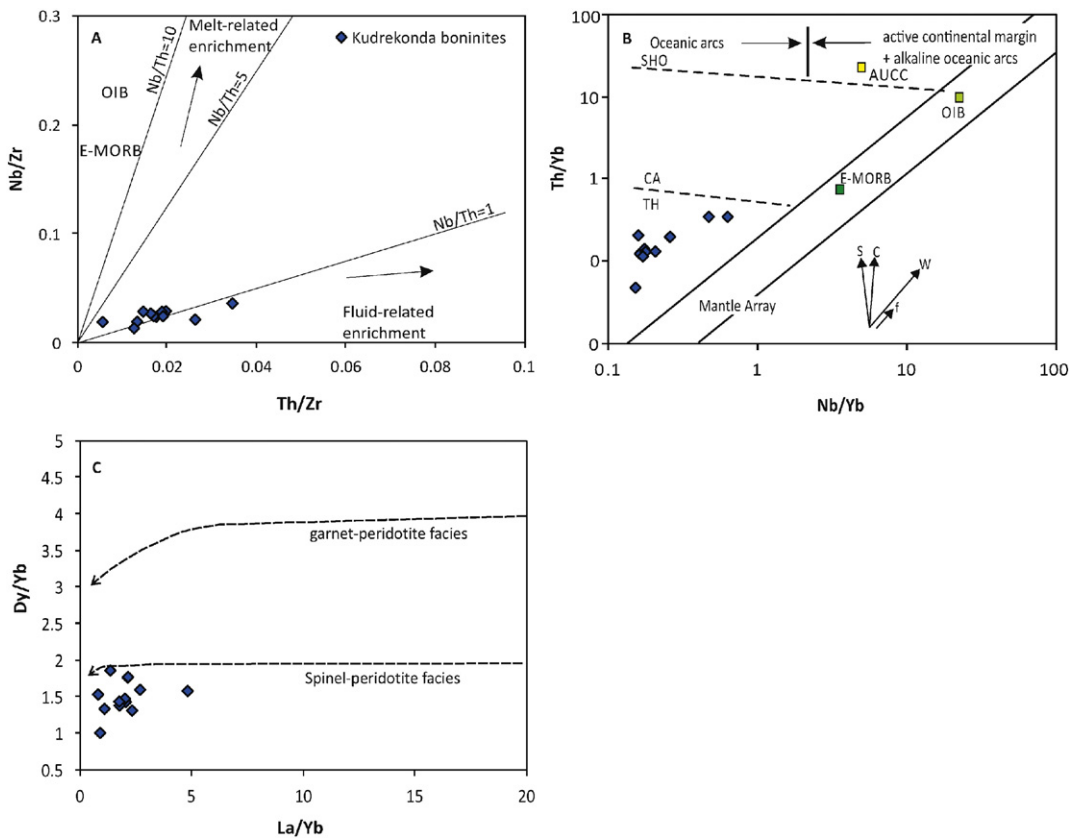


Fig. 9. (A) Nb/Zr vs. Th/Zr diagram showing the Kudrekonda boninites in an array consistent with fluid-related enrichment of mantle through subduction process. (B) Th/Yb vs. Nb/Yb plots (after Pearce (2008)) for Kudrekonda boninites showing tholeiitic lineage in the domain of oceanic island arcs. (C) Dy/Yb vs La/Yb diagram (after Rajesh et al. (2013)) suggesting mantle melting in spinel peridotite regime for Kudrekonda boninites.

2009). Based on their SiO_2 , Fe_2O_3 and Al_2O_3 contents, the BIFs have also been classified as ferruginous cherts, cherty BIFs and shaly BIFs based on relative contribution of hydrothermal solutions, volcanic and continental inputs during their deposition (Manikyamba et al., 1993). The REE geochemistry, stable and radiogenic isotopic signatures of BIFs corroborate leaching of basalts and komatiites by hydrothermal fluids in the ocean floor and subsequent mixing with bulk ferrous seawater for the generation of iron and silica in BIFs (Bau and Möller, 1993; Kato et al., 1998; Bekker et al., 2010; Wang et al., 2014). Fluctuating temperature conditions in Precambrian oceans have been advocated as one of the principal causes for alternate deposition of Si and Fe rich sediments (Posth et al., 2008). Geochemical signatures of BIFs provide important clues for understanding their depositional environment, distribution and mobility of both nutritional elements (P) and trace metals (V, Mo), chemical composition of ancient seawater, atmospheric and biospheric evolution (Beukes and Klein, 1990; Beukes et al., 1990; Kaufman et al., 1990; Bau and Möller, 1993; Bjerrum and Canfield, 2002; Konhauser et al., 2009; Pecoits et al., 2009; Wang et al., 2014).

The BIFs of Shimoga greenstone belt have low concentrations of Al_2O_3 and TiO_2 (wt.%) with marked depletion in HFSE. These geochemical features indicate minimum contributions from detrital components and negligible effect of contamination through clastic/crustal materials during precipitation. The Th/U ratio in BIF is raised by incorporation of phosphate contaminants (Wang et al., 2014). The Shimoga BIFs have low Th/U (0.4–5.2) excluding the possibility of phosphate contamination. Majority of the studied BIF samples are marked by low Th/U ratios in the range of 0.4–3.4 reflecting feeble effects of weathering, while those with higher Th/U ratios (>3.5) exhibit upper crustal weathering (Fig. 10). The PAAS-normalized REE patterns exhibit LREE depletion with positive La and Eu anomalies and superchondritic Y/Ho ratios, similar to those of modern seawater (German et al., 1995; Alibo and Nozaki,

1999). Positive Eu anomalies of these BIFs provide evidence for submarine high-T (>350 °C) hydrothermal fluid input (Bau and Dulski, 1999; Douville et al., 1999; Tang et al., 2009, 2013a,b; Zhu et al., 2015). The SiO_2 vs. Al_2O_3 diagram (Fig. 11A) suggests a genetic link of Shimoga BIFs with submarine hydrothermal activity. The elevated abundances of trace elements like Ba, Sr, V, Zn in the studied BIF samples indicate partitioning of these elements into ferric oxyhydroxides. This observation implies that these trace elements were deposited on the sea floor with ferrihydrite particles and upon burial, they were remobilized followed by resorption onto ferrous-iron containing minerals. Dymek and Klein (1988) and Klein and Beukes (1989) advocated $\Sigma(\text{Co} + \text{Cu} + \text{Ni})$ vs.

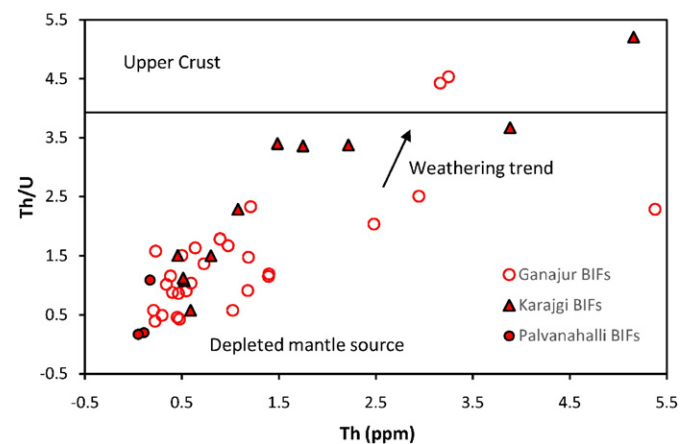


Fig. 10. Th/U vs. Th plot showing that most of the BIF samples are devoid of weathering (after McLennan et al. (1993)).

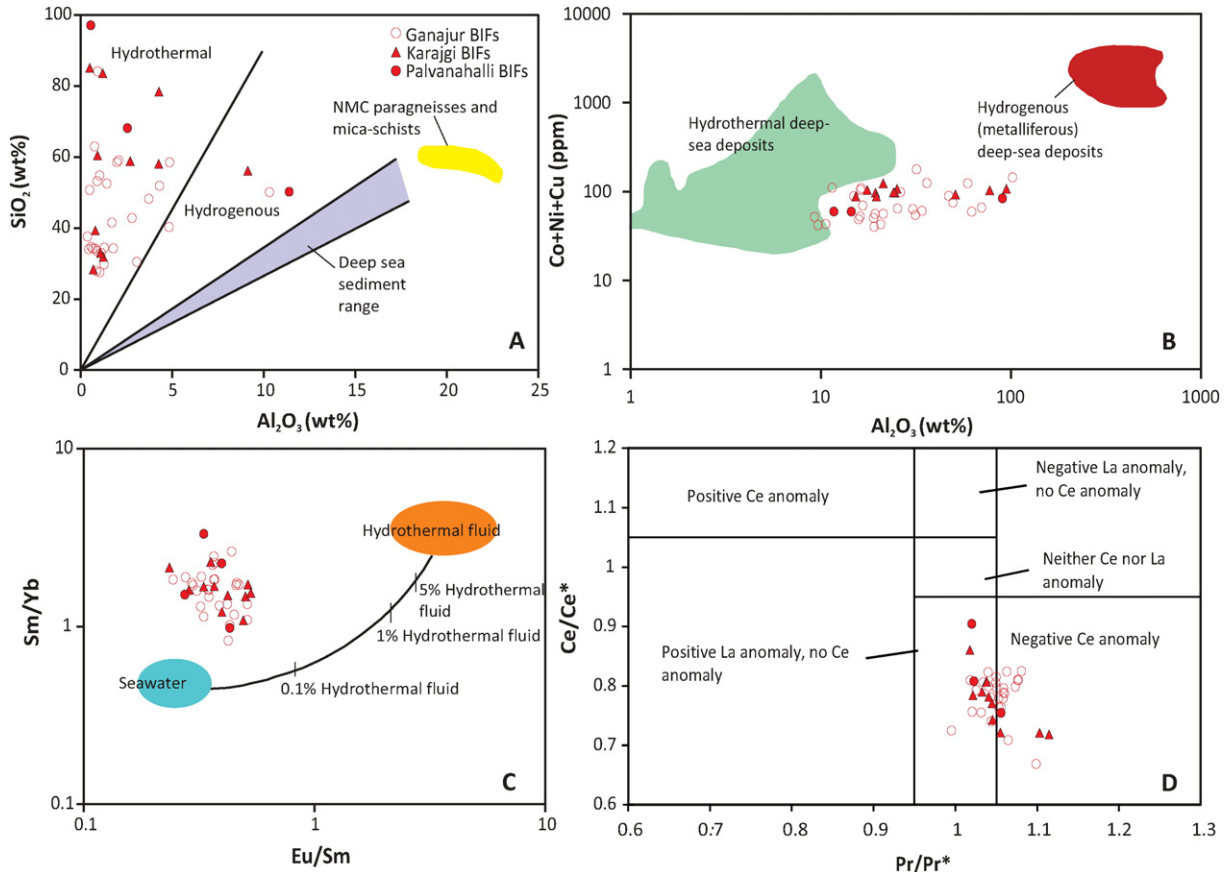


Fig. 11. (A) Al_2O_3 - SiO_2 diagram (after Zhu et al. (2015)) showing submarine hydrothermal affinity for the BIF samples. (B) $(\text{Co} + \text{Ni} + \text{Cu})$ – REE diagram (after Dymek and Klein (1988); Zhu et al. (2015)) showing most BIF samples falling within or near the field of deep sea hydrothermal deposits. (C) Sm/Yb vs. Eu/Sm plot (after Alib and Nozaki (1999)) suggesting BIF deposition from paleo-seawater with input from hydrothermal fluids (D) Ce/Ce^* and Pr/Pr^* plots (after Bau and Dulski (1996)) reflecting negligible to negative Ce anomalies for Shimoga BIFs; $[\text{Ce}/\text{Ce}^* = \text{CePAAS}/(0.5\text{LaPAAS} + 0.5\text{PrPAAS})$, $\text{Pr}/\text{Pr}^* = \text{PrPAAS}/(0.5\text{CePAAS} + 0.5\text{NdPAAS})$.

ΣREE relationship to demarcate the fields of hydrothermal and hydrogenous BIF and associated iron deposits. On $(\text{Co} + \text{Ni} + \text{Cu})$ vs. REE plot (Fig. 11B) the studied BIF samples of Shimoga cluster near the field of hydrothermal deposits. This reflects addition of iron to sea water through hydrothermal solutions from active marine environments and attests to a hydrothermal influence in the genesis of the Shimoga BIFs. According to Li et al. (2014) each silicon–iron rhythm marks a large-scale submarine hydrothermal exhalation, Fe and REEs are not fractionated during transport from exhalative centres (Bekker et al., 2010). The positive Eu anomalies of the Shimoga BIFs in combination with decreasing abundances from LREE to HREE and low Al_2O_3 contents reflect the role of high silica-low alumina hydrothermal solutions in precipitating alumina-poor iron silicates. During diagenesis, these silicates dissociate into iron hydroxide and amorphous silica which is trapped by iron oxide laminae to form bands of chert (Roy and Venkatesh, 2009). According to the depositional models for Archean BIFs (Rasmussen et al., 2013), the Fe-rich layers of Shimoga BIFs were deposited by oxidation of ferrous iron from paleo-ocean and precipitation of insoluble ferric oxyhydroxides, while the Si-rich layers were formed by removal of silica dissolved in Precambrian seawater by abiotic processes. Alexander et al. (2008) evaluated the proportion of modern seawater and high-T hydrothermal fluids through Sm/Yb - Eu/Sm relationship which indicates that extremely small amounts of submarine high-T hydrothermal fluids (~0.1%) are enough to yield strong positive Eu anomalies (Fig. 11C). According to these geochemical features, the Shimoga BIFs are considered to be the products of chemical sedimentation from paleo-seawater enriched in dissolved Fe and Si with significant input of volcanic hydrothermal fluids. Bau and Dulski (1996) proposed the Ce/Ce^* - Pr/Pr^* diagram (Fig. 11D) to identify true

Ce anomalies because positive La anomalies can create ‘false’ negative Ce anomalies. The studied BIFs plot in an array reflecting negative to no Ce anomalies (Fig. 10D) that is indicative of moderate to low atmosphere–hydrosphere redox state during BIF deposition.

A positive Eu anomaly in Archean BIFs has been interpreted as high temperature hydrothermal signature (Danielson et al., 1992). Eu anomalies in BIFs are believed to originate in the stratified oxygen-deficient bottom waters where reduction of Eu^{3+} to Eu^{2+} takes place during hydrothermal alteration of the MORB at spreading centres. The discharging hydrothermal fluid becomes enriched in Eu because of low sorption of Eu^{2+} compared to other REEs (Bau and Dulski, 1999). The pronounced positive Eu anomalies and suprachondritic Y/Ho ratios of BIFs from Ganajur, Karajgi and Palavanahalli of Shimoga greenstone belt imply distinct seawater signatures. The high Y/Ho ratios close to typical sea-water values (~44) further precludes any major dilution by detrital component (Bau and Dulski, 1999) during their deposition. The positive Eu anomalies in combination with high Y/Ho values in the Shimoga BIFs corroborate their deposition in close proximity to spreading centres. Mid-oceanic ridge-rift systems or rift controlled plume-hot spot tectonic settings are viable sites favouring release of iron that accounts for the source of Fe and Si within BIFs (Holland 1973; Morris, 1993; Alibert and McCulloch, 1993; Pirajno and Bagas, 2008; Dalstra and Rosiere, 2008; Beukes and Gutzmer 2008). It has been envisaged that hydrothermal fluids entrapped iron from Archean oceanic crust and leading to BIF formation (Polat and Frei 2005). The origin of Archean BIFs is associated with prolonged depositional episodes, variable geological conditions and depositional environments which deter any single model to explain their genesis. The Shimoga BIFs exhibit an overall depletion in ΣREE which is analogous to REE

concentrations of hydrothermal fluids and metalliferous deposits of mid-oceanic ridges (Kato et al., 1996, 1998). Hydrothermal solutions generated in present-day mid-oceanic ridge-rift systems at the East Pacific Rise (EPR), Mid-Atlantic Ridge (MAR) and Red Sea (RS) are depleted in ΣREE and have positive Eu anomalies (Derry and Jacobsen, 1990). The studied BIFs of Shimoga greenstone belt are marked by La enrichment and this is in tune with the BIFs of Archean greenstone belts from Lake Superior, Ontario and Sandur greenstone belt of Dharwar Craton (Barrett et al., 1988; Manikyamba et al., 1993). Modern sea water is generally characterized by strong negative Ce anomaly owing to Ce oxidation and removal (Elderfield and Greaves, 1982; De Baar et al., 1985). The negative to no Ce anomalies of Shimoga BIFs suggests that they were deposited in a transitional oxygenated to deoxygenated environment thereby indicating that Neoarchean sea water had variable Ce anomalies and was less oxic than modern sea water. Ce depletion and negative Ce anomalies have been documented from Jilling-Langalata BIFs of Iron Ore Group (IOG) of Singhbhum Craton (Roy and Venkatesh, 2009) and BIF of the Transvaal Supergroup, South Africa (Beukes and Klein, 1990). Negative to no Ce anomalies, depleted ΣREE and positive Eu anomalies in Shimoga BIFs collectively suggest that their metal content was added to ambient oceans by hydrothermal solutions at hydrothermally active off-shelf environment.

6.3. Genesis of gold in BIF and quartz vein hosted boninites

Hydrothermal fluids are capable of dissolving and transporting elements that are normally considered insoluble e.g. Au, Ti, Pt, owing to their chemically reactive and mobile nature under elevated temperature-pressure conditions. The generation of aqueous hydrothermal fluids is controlled by magmatic and metamorphic processes under favourable chemical and geodynamic conditions. The circulation of natural ore-forming hydrothermal fluids aids transport and deposition of elements of economic interest (Frimmel, 2008; Zhu et al., 2011). Hydrothermal gold mineralization is primarily associated with silver and base metals like Cu, Pb and Zn. Hydrothermal gold deposits are subdivided into epithermal (<5 km depth), mesothermal (>5 km depth) and hypothermal (>10 km depth) based on their depth of formation in the crust. Epigenetic gold mineralization is subsequent to host rock formation, while syngenetic gold deposits are genetically contemporaneous to their associated host rocks. Precambrian gold deposits have been classified into Witwatersrand and orogenic types; the latter is further subdivided into sediment-hosted and greenstone-hosted orogenic deposits. BIF-hosted gold deposits belong to the sediment-hosted variety and are commonly small (Gadag greenstone belt, WDC; Sarma et al., 2011, 2012), subeconomic with one exception being the Homestake BIF deposit of South Dakota, USA, which has a gold endowment of over 40 million ounces (Moz; Caddey et al., 1991; Steadman et al., 2014). Previous studies have proposed a syngenetic origin for the BIF-hosted gold deposits occurring all over the world and they have been claimed to be analogous with seafloor exhalites (Frapp, 1976; Anhaeusser, 1976; Hutchinson, 1976). However, this contention was discarded by a more viable and convincing model postulating a metamorphic-hydrothermal or epigenetic origin for the BIFs which entrapped migrating auriferous and H₂S-rich fluids (Phillips et al., 1984; Groves et al., 1987; Steadman et al., 2014).

Epithermal gold deposits including gold rich porphyry, veins and skarn deposits are related to subaerial volcanic activity and commonly occur in the shallow parts (<5 km depth) of island arcs and continental arcs in compressional and extensional tectonic regimes associated with subduction processes. Epithermal gold veins and sedimentary rock hosted Carlin-type auriferous deposits are also emplaced in shallow regions of back-arc associated with crustal thinning and extension. This type of gold mineralization occurs at temperatures ranging from 50 to 300 °C under conditions of moderate pressure within a maximum depth of 1 km but it rarely exceeds a depth of 600 m. Epithermal gold is found in veins and also form as irregular branching fissures, vesicle

fillings, stock works, breccia pipes and disseminations. The most common form of epithermal gold emplacement is open space fillings including cockscomb textures, crustifications, drusy cavities and symmetrical banding. Colloform textures, typical of a shallow volcanic environment are also common which indicate low temperatures and the free circulation of hydrothermal fluids. The associated ore assemblages include sulfantimonides, gold and silver tellurides, stibnite, cinnabar, native mercury, selenides and to a lesser extent galena, sphalerite and chalcopyrite. Epithermal gold deposits are subdivided into high sulfidation (acid sulfate) and low sulfidation (adularia-sericite) types based on the mineralizing fluids of different chemical compositions and volcanic environments that are responsible for their formation (Morishita and Nakano, 2008). The high sulfidation fluid is an oxidized and acidic fluid that originates from a magmatic source in a volcanic hydrothermal regime and deposits gold near the surface, while the low sulfidation fluid comprises a mixture of hydrothermal fluids and meteoric water (Hedenquist and Lowenstein, 1994; Heinrich, 2005). The inferences obtained on the basis of geochemical characteristics and mineral chemical data suggest that the gold occurrences in BIFs of Shimoga greenstone belt are akin to Homestake type iron-formation hosted vein and disseminated lode gold deposit deriving its name from type area in Homestake, South Dakota, USA. These BIFs are associated with volcanic, volcanoclastic and sedimentary sequences of Shimoga greenstone belt metamorphosed to greenschist to lower amphibolite facies with gold occurring in banded strata-bound disseminated sulphide lenses. The sulphide lenses consist of pyrite, pyrrhotite, arsenopyrite and native gold. Gold mineralization is attributed to hydrothermal activity and sulphidation of pre-existing iron-formation where oxides, carbonates and sulphide facies iron formation served as host rocks proximal to volcanic-sedimentary contact. Au concentration reaching up to 15,831 ppb allows these BIFs to be considered as potential host for gold mineralization. Geochemical data suggest that gold occurring in the BIF samples (L, M, N and P) are associated with Arsenic (As) and Antimony (Sb). Fig. 7 shows relative distribution of Au, As and Sb in Ganajur, Karajgi and Palavanahalli BIFs. The studied samples record high concentrations of Arsenic (As) and Antimony (Sb) implying that gold mineralization is associated with these elements which serve as potential geochemical parameters for gold exploration. The greater abundances of As relative to Sb in the BIF samples (Fig. 7 B) suggests As as a dominant tracer for gold. The immobile nature of REEs accounts for their viability as suitable indicators of source and tools for interpretation of genetic processes (Cousens et al., 1993; Sarangi et al., 2013). Therefore, REE patterns for the gold bearing BIFs of Shimoga greenstone belt reflect the nature of auriferous fluids and their source. Strong positive Eu anomalies of the BIF samples provide evidence for low oxygen fugacity conditions and reduced nature of the auriferous fluids. The oxygen-depleted auriferous fluids enriched in Eu⁺² originated in a reducing environment associated with mid-oceanic ridge-rift system and migrated to the site of BIF deposition in close proximity. Low oxygen fugacity conditions result into higher abundances of Eu⁺² over Eu⁺³ thereby giving rise to low Eu⁺³/Eu⁺². Eu⁺² preferentially combine with softer bases to precipitate and form stable complexes leading to positive Eu anomaly. Thus, it is interpreted that the gold mineralization in Shimoga BIFs is epigenetic, epithermal type and is attributed to circulation of oxygen depleted auriferous fluids of hydrothermal origin within BIFs that acted as chemical traps for the auriferous fluids. The sulphides occurring with gold in the Shimoga BIFs were derived from sulphidic fluids of hydrothermal origin that percolated the BIFs after their deposition. The auriferous-sulphidic fluids derived from mid-oceanic ridge hydrothermal activity acted as precursor for the generation of BIF-hosted gold in SGB, while syntectonic remobilization of gold during late-stage collision-accretion processes accounted for transportation and precipitation of gold in quartz veins cutting across the BIF at some places.

The mesothermal gold deposits are emplaced during compressional to transpressional tectonic activity in deformed accretionary belts adjacent to continental magmatic arcs (Groves et al., 1998, 2005; Goldfarb

et al., 2001, 2005, 2007). Mesothermal orogenic gold deposits are associated with shear zones and occur in regions that have undergone greenschist to amphibolite facies metamorphism. Mesothermal gold mineralization is spatially and genetically associated with Archaean greenstone belts and primarily hosted in mafic and ultramafic volcanic rocks, banded iron formations, greywacke and conglomerates. This type of gold mineralization occurs at moderate temperatures (200–300 °C) and pressures (~1–5 km depth) and has a huge vertical extent but a limited lateral extent. Mesothermal gold deposits are localised along or adjacent to major structural breaks or suture zones, related to collisional boundaries. Minerals associated with mesothermal gold include sulphides such as pyrite, chalcopyrite, sphalerite, galena, bornite and chalcocite. Greenstone-hosted quartz-carbonate vein type gold deposits are mesothermal, orogenic and contain pyrite, arsenopyrite, minor native gold and base metals (Hazarika et al., 2013; Sarangi et al., 2012; 2013). Most of them show abundant replacement phenomena; wall-rock alteration is characterised by quartz–pyrite–muscovite assemblages adjacent to the veins enclosed within a broader zone of carbonate alteration and altered ultramafic rocks include fuchsite or mariposite (green mica) varieties. The Kudrekonda boninites are metamorphosed to greenschist to lower amphibolite facies, show ample evidence of polyphase deformation and are cut by quartz veins associated with shear zone activities. These quartz veins containing gold grains are akin to gold occurrences in greenstone-hosted quartz-carbonate veins that are mesothermal orogenic type and particularly located in deformed and metamorphosed greenstone terranes. The studied samples (KK) show elevated concentrations of Sb with respect to As reflecting dominant role of Sb as indicator element for Au (Fig. 7). Field characteristics, petrographic features, mineral chemical and whole rock geochemical attributes infer that gold mineralization in quartz veins intruding Kudrekonda boninites are syngenetic, mesothermal conforming to a convergent margin orogenic affinity. Gold genesis was contemporaneous with the derivation of Kudrekonda boninites in intraoceanic arc setting, while the transportation and precipitation of gold in the quartz veins cutting across these boninites are ascribed to late-stage remobilization of gold during accretionary processes associated with ocean-continent collision. The generation of auriferous fluids during convergent margin magmatism invokes (i) dehydration and metamorphism of subducted oceanic lithosphere (ii) devolatilization of hydrated and metasomatized mantle wedge (e.g. Goldfarb and Santosh, 2014). It has been envisaged that the fluids responsible for transportation and precipitation of gold in greenstone-hosted quartz-vein type deposits have a hydrothermal, metamorphic origin. During accretionary processes at collisional plate margins, the volcano-sedimentary sequences are subjected to thermal re-equilibration and prograde metamorphism (Pal and Mishra, 2004; Dubé and Gosselin, 2007). The hydrothermal fluids, originating from metamorphic devolatilization reactions at deeper crustal levels, dissolve and remobilize various elements including Au during their upward migration through shear zone controlled fracture systems. These fluids serve as potential carriers of gold which gets precipitated along with sulphides within veins at higher crustal levels at favorable physico-chemical conditions (Kerrick et al., 2000; Dubé and Gosselin, 2007). Geological setting and tectonic affiliations suggest that transportation and precipitation of gold in the quartz veins of Kudrekonda boninites was governed by a similar mechanism. Hydrothermal fluids produced by devolatilization and progressive metamorphic reactions served as the most viable precursor for gold remobilization. Thus, the accretionary processes of convergent plate margins induced syntectonic remobilization of gold, while its transportation and precipitation in quartz veins was controlled by shear zone related fractures and fault systems.

The formation of orogenic gold deposits around the globe spanned over 3 billion years of the Earth's history and three distinct episodes of Precambrian orogenic gold mineralization have been recorded at 3.4–3.0 Ga, 3.0–2.5 Ga and 2.1–1.8 Ga. Orogenic gold metallogeny has been predominantly controlled by crustal growth and terrane accretion

processes along convergent plate margins. The volcano-sedimentary sequences of Archean greenstone belts from Ylgarn Craton of Australia, Zimbabwe and Tanzania Cratons of Africa, Superior Province of Canada, Slave Craton of USA and Dharwar Craton of India served as major hosts for quartz-carbonate vein type orogenic gold deposits and significant amount of the world's gold has been resourced from these terranes (Goldfarb et al., 2001; Manikyamba et al., 2014c). The latter part of the Neoarchean period (2.8–2.55 Ga) marked by hydrothermal activity, accretionary processes, juvenile crustal growth and metamorphism has been considered as an extremely favourable period for orogenic gold genesis. Gold mineralization occurring in the greenstone belts of eastern and western sectors of Dharwar Craton was predominantly controlled by metamorphic remobilization and orogenic activities. The Huttī–Jonnagiri–Kadiri–Kolar composite greenstone terrane and the Penakacherla schist belt of Ramagiri–Hungund greenstone terrane of eastern Dharwar Craton are marked by syn-orogenic, shear zone hosted gold mineralization preserving distinct signatures of Archean subduction and hydrothermal events (Manikyamba et al., 2004, 2014c, 2015). Available literature on tectonothermal history and metamorphic events of eastern Dharwar Craton suggest that gold mineralization occurred in two events between 2550 and 2530 Ma. Gold mineralization has been interpreted to be associated with assemblage of various terranes of eastern Dharwar Craton and a late to post tectonic plutonism (Kolb et al., 2005). However, the pre-peak metamorphic gold mineralization at Kolar and single stage gold mineralization at Ramagiri reflect different evolutionary history. Gold mineralization at Huttī was associated with greenschist facies metamorphism and post dates the gold mineralization of western Dharwar Craton by 35–90 Ma. U–Pb dating of detrital zircon from Gadag greenstone belt, western Dharwar Craton constrains the age of gold mineralization at 2522 ± 6 Ma (Sarma et al., 2012). U–Pb dating of monazite and xenotime from gold reefs of Gadag and Ajjannahalli gold deposits yield ages of 2522 ± 6 Ma and 2520 ± 9 Ma respectively indicating younger age of gold mineralization compared to 2.55 Ga U–Pb zircon age of hydrothermal monazite from Huttī gold deposit of eastern Dharwar Craton (Sarma et al., 2008). Gold mineralization in Ramagiri and Kolar greenstone belts is concurrent with the ages obtained for Huttī and collectively concomitant with pervasive hydrothermal activity, remobilization of auriferous fluids and cratonization of Dharwar Craton. The Shimoga greenstone belt being in the western part of Chitradurga greenstone belt collectively belong to the western Dharwar Craton and timing of quartz vein type orogenic gold mineralization associated with Kudrekonda boninites and BIF hosted gold of Ganajur, Karajgi and Palavanahalli areas of Shimoga belt appear to be geochronologically analogous to the adjacent gold deposits of Gadag and Ajjannahalli.

6.4. Geodynamic implications

A schematic illustration depicting the temporal evolution of boninites from Kudrekonda and BIFs from Ganajur, Karajgi and Palavanahalli of Shimoga greenstone belt with petrogenetic evolution of gold mineralization is given in Fig. 12. The studied lithologies were emplaced in diverse tectonic settings through distinct sedimentary and magmatic processes. The BIFs were deposited in a marine environment proximal to a mid-oceanic ridge-rift system (Stage I). Hydrothermal activity generated auriferous fluids of reducing nature under low oxygen fugacity conditions. These auriferous fluids migrated to the site of BIF deposition and circulated through the BIF during the post depositional phase. The migration and circulation of auriferous fluids of hydrothermal origin through the BIFs resulted in gold precipitation (Fig. 12). The generation of Kudrekonda boninites in a juvenile subduction zone was facilitated by subduction of hot young oceanic crust of active spreading ridge transforming to an intraoceanic arc (Stage I). Mafic volcanic rocks with boninitic signatures were derived by partial melting of a subduction-metasomatized refractory mantle wedge under hydrous conditions at shallow depth. Dehydration,

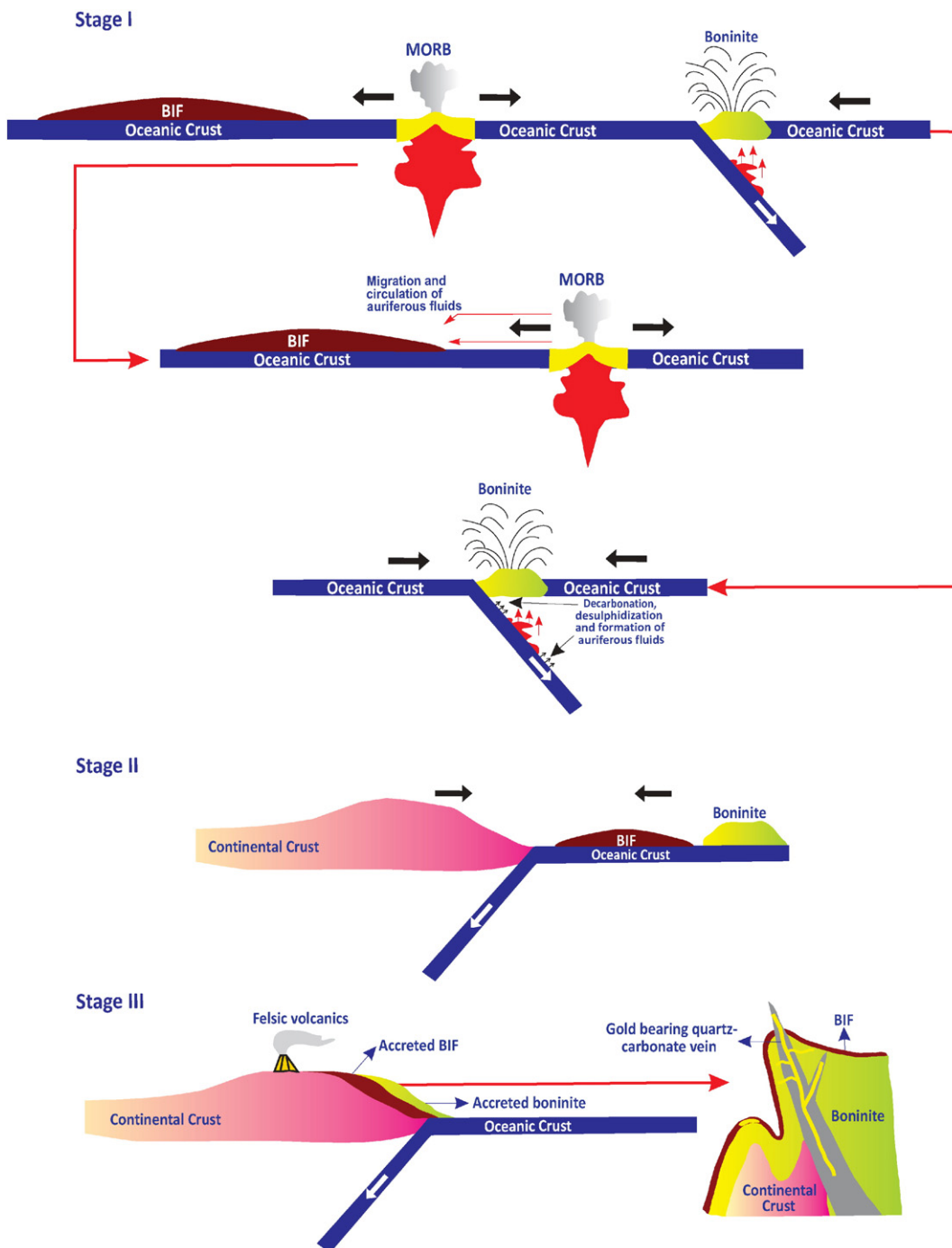


Fig. 12. A cartoon illustration showing the BIF deposition and boninite emplacement at oceanic ridge–rift system and transformation of spreading ridge to an intraoceanic arc, arc propagation towards an active continental margin and subsequent arc–continent collision and accretion.

decarbonation, desulphidization and metamorphism of subducted oceanic lithosphere coupled with devolatilization of metasomatized mantle wedge contributed to generation of auriferous fluids (Stage I). After the eruption of the boninites, the intraoceanic arc propagated towards an active continental margin (Stage II) and got accreted on the continental segment during arc–continental collision (Stage III). The hydrothermal fluids generated during accretionary process led to the remobilization of gold and its deposition in quartz–carbonate veins that cut across the boninites (Stage III). The younger felsic volcanic rocks of Shimoga derived later following the arc–continent collision through ocean–continent convergent margin processes (Stage III) marked by subduction of oceanic crust beneath continental plate with subsequent intracrustal melting (Manikyamba et al., 2014a,b).

7. Conclusions

- The geochemical signatures of the mafic volcanic rocks of Kudrekonda Formation of Shimoga greenstone belt, WDC distinguish them as boninites and suggest their generation in an intraoceanic arc setting followed by accretion to an active continental margin.
- Gold occurring within the quartz veins of Kudrekonda boninites is epigenetic with a mesothermal origin and is genetically linked with previous tectonothermal events and accretionary processes related to convergent margin activity. Hydrothermal fluids derived from devolatilization reactions during prograde metamorphism at deeper crustal levels served as potential precursor for Au precipitation.

- > The BIFs from Ganajur, Karajgi and Palavanahalli areas of Shimoga greenstone belt are silicified, carbonatized, sulfidized and their immobile trace element abundances and ratios indicate hydrothermal origin and their deposition in a marine off-shelf environment proximal to a mid-oceanic ridge-rift system.
- > The BIF hosted gold-sulphide mineralization of Shimoga greenstone belt is epigenetic, epithermal type associated with hydrothermal activity at mid-oceanic spreading centre. Auriferous hydrothermal solutions of volcanic origin were released under low oxygen fugacity conditions and these fluids migrated to the site of BIF deposition that acted as chemical traps for the sulphide rich auriferous fluids.
- > Gold in Kudrekonda boninites is genetically related to auriferous fluids of intraoceanic subduction zone, while genesis of BIF-hosted gold is attributed to hydrothermal activity at midoceanic ridge-rift system. Occurrence of gold in quartz veins cutting across Kudrekonda boninites and Karajgi BIF is interpreted as late-stage process involving syntectonic remobilization of gold, its transportation and precipitation through shear zone-controlled faults and fractures during collision-accretion at ocean-continent convergence.

Acknowledgements

The authors thank Dr. Ch Mohan Rao, Director, NGRI for permitting to publish this work. We gratefully acknowledge the editorial handling of Prof. Franco Pirajno and the constructive comments of Dr. Yener Eyboglu and an anonymous reviewer. CM acknowledges the funds from the Council of Scientific and Industrial Research (CSIR) to the National Geophysical Research Institute through the projects MLP 6201-28 (CM); and the Ministry of Earth Sciences (no: MoES/PO(Geosci)/8/2014). SG and AS acknowledge financial support from DST Inspire Faculty Projects IFA14-EAS-25 and IFA13-EAS-14 respectively. Drs. M. Satyanarayanan, S. Sawanth, K.S.V. Subramanyam and A.K. Krishna are acknowledged for providing the geochemical data. The authors express their sincere thanks to Dr. M. Korakoppa, Geologist, Geological Survey of India for his help during EPM analyses.

References

- Alexander, B.W., Bau, M., Andersson, P., Dulski, P., 2008. Continentially derived solutes in shallow Archean seawater: rare earth element and Nd isotope evidence in iron formation from the 2.9 Ga Pongola supergroup, South Africa. *Geochim. Cosmochim. Acta* 72, 378–394.
- Alibot, C., McCulloch, M.T., 1993. Rare earth element and neodymium composition of the banded iron formation and associated shales from the Hamersley, West. Aust. *Geochim. Cosmochim. Acta* 57, 187–204.
- Alibo, D.S., Nozaki, Y., 1999. Rare earth elements in seawater: particle association, shale-normalization, and Ce oxidation. *Geochim. Cosmochim. Acta* 63, 363–372.
- Anhaeusser, C.R., 1976. Archean metallogeny in Southern Africa. *Econ. Geol.* 71, 16–43.
- Arndt, N.T., 2008. *Komatiites*. Cambridge University Press, Cambridge (467 pp.).
- Barley, M.E., Eisenlohr, B.N., Groves, D.I., Perring, C.S., Vearncombe, J.R., 1989. Late Archean convergent margin tectonics and gold mineralization: A new look at the Norseman-Wiluna belt, Western Australia. *Geology* 17, 826–829.
- Barrett, T.J., Fralick, P.W., Jarvis, I., 1988. Rare-earth element geochemistry of some Archean iron formations north of Lake Superior, Ontario. *Can. J. Earth Sci.* 25, 570–580.
- Bau, M., Dulski, P., 1996. Distribution of yttrium and rare-earth elements in the Penge and Kuruman iron-formations, Transvaal supergroup, South Africa. *Precambrian Res.* 79, 37–55.
- Bau, M., Dulski, P., 1999. Comparing yttrium and rare-earth in hydrothermal fluids from the mid-Atlantic ridge: implications for Y and REE behaviour during nearvent mixing and for the Y/Ho ratio of Proterozoic seawater. *Chem. Geol.* 155, 77–90.
- Bau, M., Möller, P., 1993. Rare earth element systematics of the chemically pre-cipitated component in early Precambrian iron formations and the evolution of the terrestrial atmosphere-hydrosphere-lithosphere system. *Geochim. Cosmochim. Acta* 57, 2239–2249.
- Bekker, A., Slack, J.F., Planavsky, N., Krapež, B., Hofmann, A., Konhauser, K.O., Rouxel, O.J., 2010. Iron formation: the sedimentary product of a complex interplay among mantle, tectonic oceanic, and biospheric processes. *Econ. Geol.* 105, 467–508.
- Beukes, N.J., Gutzmer, J., 2008. Origin and paleoenvironmental significance of major iron formations at the Archean-Paleoproterozoic boundary. *Rev. Econ. Geol.* 15, 5–47.
- Beukes, N.J., Klein, C., 1990. Geochemistry and sedimentology of a facies transition from microbanded to granular iron-formation in the early Proterozoic Transvaal supergroup, South Africa. *Precambrian Res.* 47, 99–139.
- Beukes, N.J., Klein, C., Kaufmann, A.J., Hayes, J.M., 1990. Carbonate petrography, kerogen distribution, and carbon and oxygen isotopic variations in an Early Proterozoic transition from limestone to iron-formation deposition, Transvaal supergroup, South Africa. *Econ. Geol.* 85, 663–690.
- Bjerrum, C.J., Canfield, D.E., 2002. Ocean productivity before about 1.9 Gyr limited by phosphorous adsorption onto iron oxides. *Nature* 417, 159–162.
- Caddey, S.W., Bachmann, R.L., Campbell, T.J., Reid, R.R., Otto, R.P., 1991. The Home-Stake Gold Mine, an Early Proterozoic Iron-Formation-Hosted Gold Deposit, Lawrence County, South Dakota. *United States Geological Survey Bulletin*. 1857-J, pp. J1–J67.
- Chadwick, B., Vasudev, V.N., Hedge, G.V., 2000. The Dharwar craton, southern India, interpreted as the result of Late Archean oblique convergence. *Precambrian Res.* 99, 91–111.
- Chadwick, B., Vasudev, V.N., Krishna Rao, B., Hegde, G.V., 1991. The stratigraphy and structure of the Dharwar supergroup adjacent to the Honnali Dome: implications for Late Archean Basin development and regional structure in the western part of Karnataka. *J. Geol. Soc. India* 38, 457–484.
- Chardon, D., Jayananda, M., Peucat, J.-J., 2011. Lateral constrictional flow of hot orogenic crust: insights from the Neoproterozoic of South India, geological and geophysical implications for orogenic Plateaux. *Geochem. Geophys. Geosyst.* 12, Q02005. <http://dx.doi.org/10.1029/2010GC003398>.
- Cloud, P., 1965. Significance of gunflint (Precambrian) microflora. *Science* 148, 27–45.
- Condie, K.C., 2000. Episodic continental growth models: afterthoughts and extensions. *Tectonophysics* 322, 153–162.
- Cousens, B.L., Spera, F.J., Dobson, P.F., 1993. Post-eruptive alteration of silicic ignimbrites and lavas, Gran Canaria, Canary Islands: strontium, neodymium, lead and oxygen isotopic evidence. *Geochim. Cosmochim. Acta* 57, 631–640.
- Crawford, A.J., 1989. Boninites and Related Rocks. Unwin Hyman, London (465 pp.).
- Crawford, A.J., Beccaluva, L., Serri, G., 1981. Tectono-magmatic evolution of the West Philippine-Mariana region and the origin of boninites. *Earth Planet. Sci. Lett.* 54, 346–356.
- Crawford, A.J., Falloon, T.J., Green, D.H., 1989. Classification, Petrogenesis and Tectonic Setting of Boninites. In: Crawford, A.J. (Ed.), *Boninites and Related Rocks*. Unwin-Hyman, London, pp. 1–49.
- Dalstra, H., Rosière, C.A., 2008. Structural controls on high-grade iron ores hosted by banded iron formation: a global perspective. *Rev. Econ. Geol.* 15, 73–106.
- Danielson, A., Moller, P., Dulski, P., 1992. The europium anomalies in banded ironformations and the thermal history of the oceanic crust. *Chem. Geol.* 97, 89–100.
- De Baar, H.J.W., Bacon, M.P., Brewer, P.G., Bruland, K.W., 1985. Rare earth elements in the Pacific and Atlantic Oceans. *Geochim. Cosmochim. Acta* 49, 1943–1959.
- Derry, L.A., Jacobsen, S.B., 1990. The chemical evolution of Precambrian seawater: evidence from REEs in banded iron formations. *Geochim. Cosmochim. Acta* 54, 2965–2977.
- Dilek, Y., Furnes, H., 2009. Structure and geochemistry of Tethyan ophiolites and their petrogenesis in subduction rollback systems. *Lithos* 113, 1–20.
- Dilek, Y., Furnes, H., Shallo, M., 2007. Suprasubduction zone ophiolite formation along the periphery of Mesozoic Gondwana. *Gondwana Res.* 11, 453–475.
- Douville, E., Bienvenu, P., Charlou, J.L., Donval, J.P., Fouquet, Y., Appriou, P., Gamo, T., 1999. Yttrium and rare earth elements in fluids from various deep-sea hydro-thermal systems. *Geochim. Cosmochim. Acta* 63, 627–643.
- Dubé, B., Gosselin, P., 2007. Greenstone-Hosted Quartz-Carbonate Vein Deposits. In: Goodfellow, W.D. (Ed.), *Mineral Deposits of Canada: A Synthesis of Major Deposit-Types, District Metallogeny, the Evolution of Geological Provinces, and Exploration Methods*. Mineral Deposits Division, Special Publication 5. Geological Association of Canada, pp. 49–73.
- Dymek, R.F., Klein, C., 1988. Chemistry, petrology and origin of banded iron formation lithologies from the 3800 Ma Isua supracrustal belt, West Greenland. *Precambrian Res.* 39, 247–302.
- Elderfield, H., Greaves, M.J., 1982. The rare earth elements in seawater. *Nature* 296, 214–219.
- Falloon, T.J., Green, D.H., Crawford, A.J., 1987. Dredged igneous rocks from the northern termination of the Tofua magmatic arc, Tonga and adjacent Lau Basin. *Aust. J. Earth Sci.* 34, 487–506.
- Falloon, T.J., Crawford, A.J., 1991. The petrogenesis of high-calcium boninite lavas dredged from the northern Tonga ridge. *Earth Planet. Sci. Lett.* 102, 375–394.
- Falloon, T.J., Green, D.H., Danyushevsky, L.V., McNeill, A.W., 2008. The composition of near-solidus partial melts of fertile peridotite at 1 and 1.5 GPa: implications for the petrogenesis of MORB. *J. Petrol.* 49, 591–613.
- Frimmel, H.E., 2008. Earth's continental crustal gold endowment. *Earth Planet. Sci. Lett.* 267, 45–55.
- Fripp, R.E.P., 1976. Stratabound gold deposits in Archean banded iron-formation, Rhodesia. *Econ. Geol.* 71, 58–75.
- German, C.R., Masuzawa, T., Greaves, M.J., Elderfield, H., Edmond, J.M., 1995. Dissolved rare earth elements in the Southern Ocean: cerium oxidation and the influence of hydrography. *Geochim. Cosmochim. Acta* 59, 1551–1558.
- Gill, J.B., 1981. *Orogenic Andesites and Plate Tectonics*. Springer-Verlag, Berlin, Heidelberg, New York.
- Goldfarb, R.J., Baker, T., Dubé, B., Groves, D.I., Hart, C.J.R., Gosselin, P., 2005. *Distribution, Character, and Genesis of Gold Deposits in Metamorphic Terranes*. Economic Geology 100th Anniversary Volume, pp. 407–450.
- Goldfarb, R.J., Groves, D.I., Gardoll, S., 2001. Orogenic gold and geological time: a synthesis. *Ore Geol. Rev.* 18, 1–75.
- Goldfarb, R.J., Hart, C., Davis, G., 2007. East Asian gold: deciphering the anomaly of Phanerozoic gold in Precambrian cratons. *Econ. Geol.* 102, 341–345.
- Goldfarb, R.J., Snee, L.W., Pickthorn, W.J., 1993. Orogenesis, high-T thermal events, and gold vein formation within metamorphic rocks of the Alaskan Cordillera. *Mineral. Mag.* 57, 375–394.

- Goldfarb, R.J., Santosh, M., 2014. The dilemma of the Jiaodong gold deposits: are they Unique? *Geosci. Front.* 5, 139–153.
- González, P.D., Sato, A.M., Llambías, E.J., Petronilho, L.A., 2009. Petrology and geochemistry of the banded iron formation in the Eastern Sierras Pampeanas of San Luis (Argentina): implications for the evolution of the Nogolí Metamorphic Complex. *J. S. Am. Earth Sci.* 28, 89–112.
- Gross, G.A., 1996. Algoma-Type Previous Term Iron-Formation. Next Term. In: Lefebvre, D., Höy, T. (Eds.), Selected British Columbia Mineral Deposits Profiles2. Ottawa British Columbia Ministry of Employment and Investment Open File, pp. 25–28.
- Groves, D.I., Santosh, M., 2015. Province-scale commonalities of some world-class gold deposits: implications for mineral exploration. *Geosci. Front.* 6, 389–399.
- Groves, D.I., Condie, K.C., Goldfarb, R.J., Hronsky, J.M.A., 2005. Secular changes in global tectonic processes and their influence on the temporal distribution of gold-bearing mineral deposits. *Econ. Geol.* 100, 203–224.
- Groves, D.I., Goldfarb, R.J., Gebre-Mariam, M., Hagemann, S.G., Robert, F., 1998. Oro-genic gold deposits: a proposed classification in the context of their crustal distribution and relationship to other gold deposit types. *Ore Geol. Rev.* 13, 7–27.
- Groves, D.I., Goldfarb, R.J., Robert, F., Hart, C.J.R., 2003. Gold deposits in metamorphic belts: overview of current understanding, outstanding problems, future research, and exploration significance. *Econ. Geol.* 98, 1–29.
- Groves, D.I., Phillips, N., Ho, S.E., Houstoun, S.M., Standing, C.A., 1987. Craton-scaledistribution of Archean greenstone gold deposits: predictive capacity of themetamorphic model. *Econ. Geol.* 82, 2045–2058.
- Guo, P., Santosh, M., Li, S., 2013. Geodynamics of gold metallogeny in the Shandong Province, NE China: an integrated geological, geophysical and geochemical perspective. *Gondwana Res.* 24, 1172–1202.
- Harinadha Babu, P., Ponnuswamy, M., Krishna Murthy, K.V., 1981. Shimoga Belt. In: Swaminathan, J., Ramakrishnan, M. (Eds.), Early Precambrian Supracrustals of Southern Karnataka. Geological Survey of India Memoir 112, pp. 199–218.
- Hawkesworth, C.J., Turner, S.P., McDermott, F., Peate, D.W., van Calstern, P., 1997. U-Th isotopes in arc magmas: implications for element transfer from the subducted crust. *Science* 276, 551–555.
- Hazarika, P., Mishra, B., Saravanan Chinnaswamy, S., Bernhardt, H.-J., 2013. Multi-stage growth and invisible gold distribution in pyrite from the Kundarkocha sediment-hosted gold deposit, eastern India. *Ore Geol. Rev.* 55, 134–145.
- Hedenquist, J.W., Lowenstern, J.B., 1994. The role of magmas in the formation of hydrothermal ore deposits. *Nature* 370, 519–527.
- Heinrich, C.A., 2005. The physical and chemical evolution of low- to medium-salinity magmatic fluids at the porphyry to epithermal transition: a thermodynamic study. *Mineral. Deposita* 39, 864–889.
- Hole, M.J., Saunders, A.D., Marriner, G.F., Tarney, J., 1984. Subduction of pelagic sediments: implications for the origin of Ce-anomalous basalts from the Mariana Islands. *J. Geol. Soc. Lond.* 141, 453–472.
- Holland, H.D., 1973. The oceans: a possible source of iron in iron -formations. *Econ. Geol.* 68, 1169–1172.
- Holland, H.D., 2006. The oxygenation of the atmosphere and oceans. *Philos. Trans. Soc. B* 361, 903–916.
- Hutchinson, R.W., 1976. Lode Gold Deposits: The Case for Volcanogenic Distribution. Pacific Northwest Minerals and Metals Conference, Portland, Oregon, 1975, Proceedings. Department of Geology and Mineral Industries, Salem, Oregon, pp. 64–105.
- Ishizuka, O., Kimura, J.I., Li, Y.-B., Stern, R.J., Reagan, M.K., Taylor, R.N., Ohara, Y., Bloomer, S.H., Ishii, T., Hargrove III, U.S., Haraguchi, S., 2006. Early stages in the volcanism: new age, chemical and isotopic constraints. *Earth Planet. Sci. Lett.* 250, 385–401.
- Ishizuka, O., Tani, K., Reagan, M.K., Kanayama, K., Umino, S., Harigane, Y., Sakamoto, I., Miyajima, Y., Yuasa, M., Dunkley, D.J., 2011. The timescales of subduction initiation and subsequent evolution of an oceanic island arc. *Earth Planet. Sci. Lett.* 306, 229–240.
- Isley, A.E., Abbott, D.H., 1999. Plume-related mafic volcanism and the deposition of banded iron formation. *J. Geophys. Res.* 104, 15461–15477.
- Jayananda, M., Chardon, D., Peucat, J.J., Capdevila, R., Martin, H., 2006. 2.61 Ga potassic granites and crustal reworking, western Dharwar Craton (India): tectonic, geochronologic and geochemical constraints. *Precambrian Res.* 150, 1–26.
- Jayananda, M., Kano, T., Peucat, J.-J., Channabasappa, S., 2008. 3.35 Ga komatiite volcanism in the western Dharwar craton, southern India: constraints from Nd isotopes and whole-rock geochemistry. *Precambrian Res.* 162, 160–179.
- Jayananda, M., Peucat, J.-J., Chardon, D., Krishna Rao, B., Fanning, C.M., Corfu, F., 2013a. Neoarchean greenstone volcanism and continental growth, Dharwar Craton, southern India: constraints from SIMS U-Pb zircon geochronology and Nd isotopes. *Precambrian Res.* 227, 55–76.
- Jayananda, M., Tsutsumi, Y., Miyazaki, T., Gireesh, R.V., Kapfo, K.-u., Tussipokla Hirossi, H., Kano, T., 2013b. Geochronological constraints on Meso and Neoarchean regional metamorphism in the Dharwar Craton, southern India. *J. Asian Earth Sci.* <http://dx.doi.org/10.1016/j.jseas.2013.04.033>.
- Kappler, A., Pasquero, C., Konhauser, K.O., Newman, D.K., 2005. Deposition of banded iron formations by anoxygenic phototrophic Fe(II)-oxidizing bacteria. *Bull. Geol. Soc. Am.* 33, 865–868.
- Kasting, J.F., 1993. Earth's early atmosphere. *Science* 259, 920–926.
- Kato, Y., Kawakami, T., Kano, T., Kunugiza, K., Swamy, N.S., 1996. Rare-earth element geochemistry of banded iron formations and associated amphibolite from the Sargur belts. South India; *J. SE Asian Earth Sci.* 14, 161–164.
- Kato, Y., Ohta, I., Tsunematsu, T., Watanabe, Y., Isozaki, Y., Maruyama, S., Imai, N., 1998. Rare earth element variations in mid-Archean banded iron formations: implications for the chemistry of ocean and continent and plate tectonics. *Geochim. Cosmochim. Acta* 62, 3475–3497.
- Kaufman, A.J., Hayes, J.M., Klein, C., 1990. Primary and diagenetic controls of isotopic compositions of iron-formation carbonates. *Geochim. Cosmochim. Acta* 54, 3461–3473.
- Kerrick, R., Goldfarb, R., Groves, D., Garwin, S., 2000. The Geodynamic of World-Class Gold Deposits: Characteristics, Space-Time Distribution and Origins. In: Hagemann, S.G., Brown, P.E. (Eds.), *Gold in 2000: Society of Economic Geologists. Rev. Econ. Geol.* 13, pp. 501–551.
- Kerrick, R., Wyman, D., Fan, J., Bleeker, W., 1998. Boninite series: low Ti-tholeiite association from the 2.7 Ga Abitibi greenstone belt. *Earth Planet. Sci. Lett.* 164, 303–316.
- Kerrick, R., Wyman, D.A., 1990. Geodynamic setting of mesothermal gold deposits: an association with accretionary tectonic regimes. *Geology* 18, 882–885.
- Klein, C., 2005. Some Precambrian banded iron-formations (BIFs) from around theworld: their age, geologic setting, mineralogy, metamorphism, geochemistry, and origins. *Am. Mineral.* 90, 1473–1499.
- Klein, C., Beukes, N.J., 1989. Geochemistry and sedimentology of a facies transition from limestone to iron-formation deposition in the Early Proterozoic Transvaal supergroup, South Africa. *Econ. Geol.* 84, 1733–1774.
- Kolb, J., Rogers, A., Michael Meyer, F., 2005. Relative timing of deformation and two stage gold mineralization at the Hutti mine, Dharwar Craton, India. *Mineral. Deposita* 40, 156–174.
- Konhauser, K.O., Hamade, T., Raiswell, R., Morris, R.C., Grant, F.F., Southam, G., Canfield, D.E., 2002. Could bacteria have formed the Precambrian banded iron formations? *Geol. Soc. Am.* 30, 079–1082.
- Konhauser, K.O., Pecoits, E., Lalonde, S.V., Papineau, D., Nisbet, E.G., Barley, M.E., Arndt, N.T., Zahnle, K., Kamber, B.S., 2009. Oceanic nickel depletion and amethanogen famine before the great oxidation event. *Nature* 458, 750–753.
- Konig, S., Munker, C., Schuth, S., Luguet, A., Hoffmann, J.E., Kudouon, J., 2010. Boninites as windows into trace element mobility in subduction zones. *Geochim. Cosmochim. Acta* 74, 684–704.
- Krishna, A.K., Murthy, N.N., Govil, P.K., 2007. Multielement analysis of soils by wavelength-dispersive X-ray fluorescence spectrometry. *At. Spectrosc.* 28, 202–215.
- Kumar, A., Bhaskar Rao, Y.J., Sivaraman, T.V., Gopalan, K., 1996. Sm–Nd agesof Archean metavolcanic of the Dharwar Craton, South India. *Precambrian Res.* 80, 206–215.
- Le Bas, M.J., 2000. IUGS reclassification of the high-Mg and picritic volcanic rocks. *J. Petrol.* 41, 1467–1470.
- Li, S.R., Santosh, M., 2013. Metallogeny and craton destruction: records from the North China Craton. *Ore Geol. Rev.* <http://dx.doi.org/10.1016/j.oregeorev.2013.03.002>.
- Li, Q., Zhang, Z., Geng, X., Li, C., Liu, F., Chai, F., Yang, F., 2014. Geology and geochemistry of the qiaoxialala Fe–Cu–Au deposit, Junggar region, northwest China. *Ore Geol. Rev.* 57, 462–481.
- Lingadevaru, M., Shadakshara Swamy 8, Anantha Murthy, K.S., Mahabaleswar, B., 2007. Metamorphic P – T conditions of Hanur granites, Karnataka, Southern India. *Kuvempu Univ. Sci. J.* 4, 123–131.
- Manikyamba, C., 2000. Transtratonic shear zones and gold mineralization – an example from Penakacherla schist belt. *Visakha Sci. J. Andhra Pradesh Acad. Sci.* 4, 1–12.
- Manikyamba, C., Balaram, V., Naqvi, S.M., 1993. Geochemical signatures of polygeneticity of banded iron formations (BIF) of Archean greenstone belt (Schist belt) Karnataka Nucleus, India. *Precambrian Res.* 61, 137–164.
- Manikyamba, C., Naqvi, S.M., Sawkar, R.H., G.R. Group, 1997. Identification of Sandur schist belt as a potential gold field. *Curr. Sci.* 72, 515–518.
- Manikyamba, C., Naqvi, S.M., Ram Mohan, M., Gnaneswar Rao, T., 2004. Gold mineralisation and alteration of Penakacherla schist belt, India, constraints on Archaean subduction and fluid processes. *Ore Geol. Rev.* 24, 199–227.
- Manikyamba, C., Naqvi, S.M., Rao, D.V.S., Mohan, M.R., Khanna, T.C., Rao, T.G., Reddy, G.L.N., 2005. Boninites from the Neoarchean Gadwal greenstone belt, eastern Dharwar Craton, India: implications for Archean subduction processes. *Earth Planet. Sci. Lett.* 230, 65–83.
- Manikyamba, C., Konrich, R., Polat, A., Saha, A., 2013. Geochemistry of two stratigraphically-related ultramafic (komatiite) layers from the Neoarchean Sigegudda greenstone terrane, Western Dharwar Craton, India: evidence for compositional diversity in Archean mantle plumes. *Lithos* 177, 120–135.
- Manikyamba, C., Ganguly, S., Saha, A., Santosh, M., Singh, M.R., Subba Rao, D.V., 2014a. Continental lithospheric evolution: constraints from the geochemistry of felsic volcanic rocks in the Dharwar Craton, India. *J. Asian Earth Sci.* 95, 65–80.
- Manikyamba, C., Saha, A., Santosh, M., Ganguly, S., Singh, M.R., Subba Rao, D.V., 2014b. Neoarchean felsic volcanic rocks from the Shimoga greenstone belt, Dharwar Craton, India: geochemical fingerprints of crustal growth at an active continental margin. *Precambrian Res.* 252, 1–21.
- Manikyamba, C., Saha, A., Ganguly, S., Santosh, M., Lingadevaru, M., Rajanikanta Singh, M., Subba Rao, D.V., 2014c. Sediment-infill volcanic breccia from the Neoarchean himoga greenstone terrane, western Dharwar craton: implications on pyroclastic volcanism and sedimentation in an active continental margin. *J. Asian Earth Sci.* 96, 269–278.
- Manikyamba, C., Ganguly, S., Santosh, M., Saha, A., Chatterjee, A., Khelen, A.C., 2015. Neoarchean arc-juvenile back-arc magmatism in eastern Dharwar Craton, India: geochemical fingerprints from the basalts of Kadiri greenstone belt. *Precambrian Res.* 258, 1–23.
- McLennan, S.M., Hemming, S., McDaniel, D.K., Hanson, G.N., 1993. Geochemical approaches to sedimentation, provenance, and tectonics. *Geol. Soc. Am. Spec. Pap.* 284, 21–40.
- Meffre, S., Aitchison, J.C., Crawford, A.J., 1996. Geochemical stratigraphy of boninites and tholeiites from the Permo-Triassic Koh Ophiolite, New Caledonia. *Tectonics* 15, 67–83.
- Morishita, Y., Nakano, T., 2008. Role of basement in epithermal deposits: the Kushikino and Hishikari gold deposits, southwestern Japan. *Ore Geol. Rev.* 34, 597–609.
- Morris, R.C., 1993. Genetic modeling for banded iron-formations of the Hamersley Group, Pilbara Craton, Western Australia. *Precambrian Res.* 60, 243–286.
- Moyen, J.-F., Martin, H., Jayananda, M., Auvray, B., 2003. Late Archean granites: a typology based on the Dharwar Craton (India). *Precambrian Res.* 127, 103–123.
- Naqvi, S.M., 2005. *Geology and Evolution of the Indian Plate (From Hadean to Holocene – 4 Ga to 4 Ka)*. Capital Publishing Company, New Delhi (450 pp.).

- Naqvi, S.M., Rogers, J.J.W., 1987. Precambrian Geology of India. Oxford Monographs on Geology and Geophysics. Oxford University Press, Oxford (223 pp.).
- Naqvi, S.M., Charan, S.N., Uday Raj, B., Hussain, S.M., Subba Rao, D.V., Balaram, V., Natarajan, R., Govil, P.K., Mathur, R., Manikyamba, C., et al., 1998. Gold Mineralization and Exploitation in the BIF of Chitradurga and Sandur Schist Belts. Golden Jubilee Souvenir. Hutt Gold Mines Comp. Ltd, pp. 64–79.
- Naqvi, S.M., Charan, S.N., Hussain, T.S.M., Uday Raj, B., Subba Rao, D.V., Manikyamba, C., Sunder Raju, P.V., Sarma, D.S., Ram Mohan, M., 1999. Sulphide Banded Iron Formations – Most Promising Target for Open Cast Mining for Gold. Proceedings of the National Conference on Mineral Informatics. Geological Society of India, Bangalore, pp. 98–118.
- O'Neil, J., Franscis, D., Carlson, R.W., 2011. Implications of the Nuvvuaguitq green-stone belt for the formation of Earth's early crust. *J. Petrol.* 52, 985–1009.
- O'Neil, J., Franscis, D., Carlson, R.W., 2012. Formation age and metamorphic history of the Nuvvuaguitq Greenstone Belt. *Precambrian Res.* 220, 23–44.
- Pal, N., Mishra, B.M., 2004. Epigenetic nature of BIF-hosted gold mineralization at Ajjannahalli, southern India: evidence from ore petrography and fluid inclusion studies. *Gondwana Res.* 6, 531–540.
- Pearce, J.A., 2008. Geochemical fingerprinting of oceanic basalts with applications to ophiolite classification and the search for Archean oceanic crust. *Lithos* 100, 14–48.
- Pearce, J.A., Vander Laan, S.R., Arculus, R.J., Murton, B.J., Ishii, T., Peate, D.W., Parkinson, I.J., 1992. Boninite and harzburgite from Leg 125 (Bonin–Mariana forearc): a case study of magma genesis during the initial stages of subduction, in Fryer. *Proc. Ocean Drill. Program Sci. Results* 125, 623–659.
- Pecotis, E., Gingras, M.K., Barley, M.E., Kappler, A., Posth, N.R., Konhauser, K.O., 2009. Petrography and geochemistry of the Dales Gorge banded iron formation: paragenetic sequence, source and implications for palaeo-ocean chemistry. *Precambrian Res.* 172, 163–187.
- Perfit, M.R., Gust, D.A., Bence, A.E., Arculus, R.J., Taylor, S.R., 1980. Chemical characteristics of island-arc basalts: implications for mantle sources. *Chem. Geol.* 30, 227–256.
- Phillips, G.N., 1991. Gold deposits of Victoria: a major province within a Palaeozoic sedimentary succession. *World Gold 91*. Aust. Inst. Min. Meta Univ., 237–245 Melbourne.
- Phillips, G.N., Groves, D.I., Martyn, J.E., 1984. An epigenetic origin for Archean banded-iron-formation-hosted gold deposits. *Econ. Geol.* 79, 162–171.
- Piercey, S.J., Murphy, D.C., Mortensen, J.K., Paradis, S., 2001. Boninitic magmatism in a continental margin setting, Yukon–Tanana terrane, southeastern Yukon, Canada. *Geology* 29 (8), 731–734.
- Pirajno, F., Bagas, L., 2008. A review of Australia's Proterozoic mineral systems and genetic models. *Precambrian Res.* 166, 54–80.
- Poidevin, J.L., 1994. Boninite-like rocks from the Palaeoproterozoic greenstone belt of Bogoin, Central African Republic: geochemistry and petrogenesis. *Precambrian Res.* 68, 97–113.
- Polat, A., Frei, R., 2005. The origin of early Archean banded iron formations and of continental crust, Isua, southern West Greenland. *Precambrian Res.* 138, 151–175.
- Polat, A., Hofmann, A.W., Rosing, M.T., 2002. Boninite-like volcanic rocks in the 3.7–3.8 Ga Isua greenstone belt, West Greenland: geochemical evidence for intra-oceanic subduction zone processes in the early Earth. *Chem. Geol.* 184, 231–254.
- Posth, N.R., Hegler, F., Konhauser, K.O., Kappler, A., 2008. Alternating Si and Fe deposition caused by temperature fluctuations in Precambrian oceans. *Nat. Geosci.* 1, 703–708.
- Powell, R., Will, T.M., Phillips, G.N., 1991. Metamorphism in Archean greenstone belts: calculated fluid compositions and implications for gold mineralization. *J. Metamorph. Geol.* 9, 141–150.
- Radhakrishna, B.P., Curtis, L.C., 1991. Gold: the Indian scene. *Mineral resources of India 3. Geol. Soc. India* 19–41.
- Radhakrishna, B.P., Curtis, L.C., 1999. Gold in India: Bangalore. Geological Society of India Economic Geology Series 7 (307 pp.).
- Radhakrishna, B.P., 1940. Note on Talya Conglomerate. 37. Records of Mysore Geology Department, pp. 135–136.
- Radhakrishna, B.P., 1941. Notes on Prospecting Alluvial Gold Around Kudrekonda and Palavanhalli, Honali Taluk, Shimoga District. 39. Records of Mysore Geological Department, pp. 160–179.
- Rajesh, H.M., Chisonga, B.C., Shindo, K., Beukes, N.J., Armstrong, R.A., 2013. Petrographic, geochemical and SHRIMP U–Pb titanite age characterization of the Thabazimbi mafic sills: extended time frame and a unifying petrogenetic model for the Bushveld Large Igneous Province. *Precambrian Res.* 230, 79–102.
- Rama Rao, B., 1963. Gold occurrences in Mysore and their prospects for large scale exploration. *Mem. Geol. Soc. India* 1, 21–30.
- Ramakrishnan, M., Vaidyanadhan, R., 2010. Geology of India. Geol. Soc. India, Bangalore, 1 (556 pp.).
- Rasmussen, B., Meier, D.B., Krapez, B., Muhling, J.R., 2013. Iron silicate microgranules as precursor sediments to 2.5-billion-year-old banded iron formations. *Geology* 41, 435–438.
- Robert, F., Poulsen, K.H., Dubé, B., 1997. Gold Deposits and Their Geological Classification. In: Gubins, A.G. (Ed.), *Proceedings of Exploration'97: Fourth Decennial International Conference on Mineral Exploration*, pp. 209–220.
- Rogers, N.W., MacLeod, C.J., Murton, B.J., 1989. Petrogenesis of Boninitic Lavas from Limassol Forest Complex, Cyprus. In: Crawford, A.J. (Ed.), Boninites. University of Tasmania, Geology Department, Hobart, Tasmania, pp. 288–311.
- Rollinson, H.R., 1993. Using Geochemical Data: Evolution, Presentation, Interpretation. Longman Group UK Limited, Singapore.
- Roy, S., Venkatesh, A.S., 2009. Mineralogy and geochemistry of banded iron formation and iron ores from eastern India with implications on their genesis. *J. Earth Syst. Sci.* 118, 619–641.
- Rubin, K.H., Sinton, J.M., MacLennan, J., Hellebrand, E., 2009. Magmatic filtering of mantle compositions at mid-ocean ridge volcanoes. *Nat. Geosci.* 2, 321–328.
- Santosh, M., Omana, P.K., 1991. Very high purity gold form lateritic weathering profiles of Nilambur, southern India. *Geology* 19, 746–749.
- Sarangi, S., Sarkar, A., Srinivasan, R., Patel, S.C., 2012. Carbon isotope studies of auriferous quartz carbonate veins from two orogenic gold deposits from the Neoproterozoic Chitradurga schist belt, Dharwar craton, India: evidence for mantle/magmatic source of auriferous fluid. *J. Asian Earth Sci.* 52, 1–11.
- Sarangi, S., Srinivasan, R., Balaram, V., 2013. REE geochemistry of auriferous quartz carbonate veins of Neoarchean Ajjannahalli gold deposit, Chitradurga schist belt, Dharwar Craton, India. *Econ. Geol.* 4, 231–239.
- Sarma, D.S., McNaughton, N.J., Fletcher, I.R., Groves, D.I., Ram Mohan, M., Balaram, V., 2008. Timing of gold mineralization in the Hutt gold deposit, Dharwar Craton, south India. *Econ. Geol.* 103, 1715–1727.
- Sarma, D.S., Fletcher, I.R., Rasmussen, B., McNaughton, N.J., Ram Mohan, M., Groves, D.I., 2011. Archaean gold mineralization synchronous with late cratonization of the Western Dharwar Craton, India: 2.52 Ga U–Pb ages of hydrothermal monazite and xenotime in gold deposits. *Mineral. Deposita* 46, 273–288.
- Sarma, D.S., McNaughton, N.J., Belusova, E., Ram Mohan, M., Fletcher, I.R., 2012. Detrital zircon U–Pb ages and Hf-isotope systematics from the Gadag Greenstone Belt: Archean crustal growth in the western Dharwar Craton, India. *Gondwana Res.* 22, 843–854.
- Smithies, R.H., 2002. Archean boninite-like rocks in an intracratonic setting. *Earth Planet. Sci. Lett.* 197, 19–34.
- Smithies, R.H., Champion, D.C., Sun, S.-S., 2004. The case of Archean boninites. *Contrib. Mineral. Petr.* 147, 705–721.
- Sproule, R.A., Lesher, C.M., Ayer, J.A., Thurston, P.C., Herzberg, C.T., 2002. Spatial and temporal variations in the geochemistry of komatiites and komatitic basalts in the Abitibi Greenstone Belt. *Precambrian Res.* 115, 153–186.
- Steadman, J.A., Large, R.R., Davidson, G.J., Bull, S.W., Thompson, J., Ireland, T.R., Holden, P., 2014. Paragenesis and composition of ore minerals in the RandallsBIF-hosted gold deposits, Yilgarn craton, Western Australia: implications for the timing of deposit formation and constraint on gold sources. *Precambrian Res.* 243, 110–132.
- Stern, R.J., Morris, J., Bloomer, S.H., Hawkins Jr., J.W., 1991. The source of metasomatic fluids and the generation of arc melts: Trace element and radiogenic isotope evidence from Eocene boninites, Mariana forearc. *Geochim. Cosmochim. Acta* 55, 1467–1481.
- Stern, R.J., Reagan, M., Ishizuka, O., Ohara, Y., Whattam, S., 2012. To understand subduction initiation, study forearc crust; to understand forearc crust, study ophiolites. *Lithosphere* 4, 469–483.
- Stiegler, M.T., Cooper, M., Byerly, G.R., Lowe, D.R., 2012. Geochemistry and petrology of komatiites of the Pioneer Ultramafic Complex of the 3.3 Ga Weltevreden Formation, Barberton greenstone belt, South Africa. *Precambrian Res.* 212–213, 1–12.
- Sun, S.S., McDonough, W.F., 1989. Chemical and Isotopic Systematics of Oceanic Basalts, Implications for Mantle Composition and Processes. In: Saunders, A.D., Norry, M.J. (Eds.), *Migmatism in the Ocean Basins*. Geol. Soc. Lond. Spec. Publ. 42, pp. 313–345.
- Swami Nath, J., Ramakrishnan, M., 1981. The Early Precambrian supracrustals of southern Karnataka. *Mem. Geol. Surv. India* 112 (350 pp.).
- Tang, H.S., Chen, Y.J., Santosh, M., Zhong, H., Wu, G., Lai, Y., 2013a. C–O isotopegeochemistry of the Dashiqiao magneisite belt, North China Craton: implications for the Great Oxidation Event and ore genesis. *Geol. J.* 48, 467–483.
- Tang, H.S., Chen, Y.J., Santosh, M., Zhong, H., Yang, T., 2013b. REE geochemistry of carbonates from the Guanmenshan Formation, Liaohe Group, NE Sino-Korean Craton: implications for seawater compositional change during the Great Oxidation Event. *Precambrian Res.* 227, 316–336.
- Tang, H.S., Chen, Y.J., Wu, G., Yang, T., 2009. Rare earth element geochemistry of carbonates of Dashiqiao Formation, Liaohe Group, eastern Liaoning Province: implication for Lomagundi Event. *Acta Petrol. Sin.* 25, 3075–3093 (in Chinese with English abstract).
- Trendall, A.F., de Laeter, J.R., Nelson, D.R., Bhaskar Rao, Y.J., 1997a. Further zircon U–Pb age data for the Daginkatte formation, Dharwar supergroup, Karnataka craton. *J. Geol. Soc. India* 50, 25–30.
- Trendall, A.F., de Laeter, J.R., Nelson, D.R., Mukhopadhyay, D., 1997b. A precise U–Pb age for the base of Mulaingiri formation (Bababudan Group, Dharwar Supergroup) of the Karnataka craton. *J. Geol. Soc. India* 50, 161–170.
- Turner, S., Rushmer, T., Reagan, M., Moyen, J.-F., 2014. Heading down early on? Starton subduction on Earth. *Geology* 42, 139–142.
- Wang, C., Zhang, L., Lan, C., Dai, Y., 2014. Petrology and geochemistry of the Wangjiazhuang banded ironformation and associated supracrustal rocks from the Wutaigreenstone belt in the North China Craton: Implications for their origin and tectonic setting. *Precambrian Res.* 255, 603–626.
- Winchester, J.A., Floyd, P.A., 1977. Geochemical discrimination of different magma series and their differentiation products using immobile elements. *Chem. Geol.* 20, 325–343.
- Wyman, D.A., 1999. Paleoproterozoic boninites in an ophiolite-like setting, trans-Hudson orogen, Canada. *Geology* 27, 455–458.
- Xia, X., Song, S., Niu, Y., 2012. Tholeiite–boninite terrane in the north Qilian suture zone: implications for subduction initiation and back-arc basin development. *Chem. Geol.* 328, 259–277.
- Yang, Q., Santosh, M., Shen, J., Li, S., 2014. Juvenile vs. recycled crust in NE China: zircon U–Pb geochronology, Hf isotope and an integrated model for Mesozoic gold mineralization in the Jiaodong Peninsula. *Gondwana Res.* 25, 1445–1468.
- Zhai, M.G., Santosh, M., 2013. Metallogeny of the North China Craton: link with secular changes in the evolving Earth. *Gondwana Res.* 24, 275–297.
- Zhu, M., Dai, Y., Zhang, L., Wang, C., Liu, L., 2015. Geochronology and geochemistry of the Nanfen iron deposit in the Anshan–Benxi area, North China Craton: implications for ~2.55 Ga crustal growth and the genesis of high-grade iron ores. *Precambrian Res.* 260, 23–38.
- Zhu, Y., An, F., Tan, J., 2011. Geochemistry of hydrothermal gold deposits: a review. *Geosci. Front.* 2, 367–374.